# Magnetic grain-size analyses of Holocene sediments in the North Atlantic and Norwegian Sea – palaeoceano-graphic applications

*Torbjörn Wall*

Examensarbeten i Geologi vid
Lunds universitet - Kvartärgeologi, nr. 179

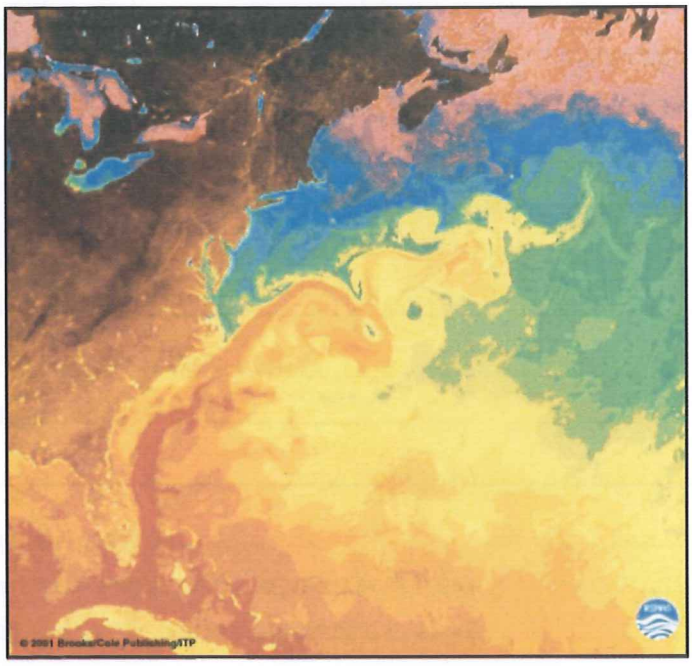

Geologiska institutionen
Centrum för GeoBiosfärsvetenskap
Lunds universitet
2004

kilo

# Magnetic grain-size analyses of Holocene sediments in the North Atlantic and Norwegian Sea - palaeoceanographic applications

**Torbjörn Wall**

Wall, Torbjörn, 2004: Magnetic grain-size analyses of Holocene sediments in the North Atlantic and Norwegian Sea - palaeoceanographic applications. *Examensarbete i Geologi vid Lunds Universitet – Kvartärgeologi, nr 179.*

**Abstract**

High-resolution magnetic hysteresis measurements were carried out on three sediment cores, one from the North Atlantic and two from the Norwegian Sea. These measurements can be used to reconstruct changes in magnetic grain-size. Physical grain-size has been interpreted as a proxy for bottom current intensity (McCave *et al.* 1995) and this study shows that the hysteresis measurements can contribute as a proxy for near bottom currents in this region during the Holocene, but only when the magnetic measurements are combined with other proxy records. The magnetic grain-size record of one core from the Norwegian Sea has been compared with sea surface temperature reconstructions produced by Calvo *et al.* (2002) and Birks & Koç (2002). The dominant magnetic mineral in the sediment is low titanium content magnetite (titanomagnetite) and the grain-size variation is discussed as a potential of near-bottom current flow intensity during the Holocene. A core from the Vøring plateau (MD95-2011) shows that the magnetic grain-size has a significant positive correlation to SST during the Holocene. Maximum sediment grain-size was reached between 9000 to 6000 cal BP, which would imply that the THC was most active in the Norwegian Sea during the Holocene thermal maximum, as registered by SST and terrestrial reconstructions. The core LO09-14 on the Reykjanes Ridge in the North Atlantic shows the same behaviour during the first part of the Holocene, but after 7500 cal BP there are indications of a shift in the oceanographic conditions and at 3700 cal BP the magnetic mineral sediment source changed and the magnetic properties cannot be used to reconstruct near-bottom current flow intensity. Core M23258-2 from south of Svalbard does not show the same behaviour at all and the variable magnetic properties of the core appear to be dominated by ice-rafted-debris.

**Keywords**: Magnetic grain-size, Magnetic hysteresis loops, Reykjanes Ridge, Vøring plateau, North Atlantic, Norwegian Sea, Deep ocean currents, Holocene.

Torbjörn Wall, Department of Geology, GeoBiosphere Science Centre, University of Lund, Sölvegatan 12, 223 62 Lund, Sweden.

# Magnetisk kornstorleksanalys av Holocena sediment från Nordatlanten och Norska havet - palaeoceanografisk tillämpning

Wall, Torbjörn, 2004: Magnetisk kornstorleksanalys av Holocena sediment från Nordatlanten och Norska havet - palaeoceanografisk tillämpning. *Examensarbete i Geologi vid Lunds Universitet – Kvartärgeologi, nr 179*

**Sammanfattning**
Mätningar av magnetisk hysteresis har genomförts på sedimentborrkärnor med hög tidsupplösning för att studera om sedimentkornstorleken kan relateras till relativ bottenströmshastighet. Mätningarna utfördes på tre borrkärnor, en från Nordatlanten och två från Norska havet. Hysteresismätningar är känsliga för variationer i de magnetiska kornstorlekarna (Day *et al.* 1977) och anses vara representativa för medelkornstorleken i ett sediment (Snowball and Moros 2003). De magnetiska mineralen i bottensedimentet är lågthaltig titanmagnetit (titanomagnetite). Fysiska kornstorlekar har tidigare använts för rekonstruktion av bottenströmmar (McCave *et al.* 1995) och magnetiska kornstorleksvariationerna har tolkats som en indikation för bottenströmstyrka under Holocen. Kärnan från Vøringplatån (MD95-2011) i Norska havet visar att den magnetiska kornstorleksvariationen har en signifikant korrelation med ytvattentemperaturen i samma område under Holocen (Calvo *et al.* 2002). Mellan 9,000 till 6,000 kalibrerade år BP (innan 1950) når den magnetiska kornstorleken sitt maximum, vilket sker samtidigt som havsytetemperaturen når sitt maximum, troligtvis då den termohalina cirkulationen (THC) var som mest effektiv i Norska havet (Andersen *et al.* 2004). Borrkärnan från Reykjanesryggen (LO09-14) i Nordatlanten uppvisar liknande mönster under första delen av Holocen. Efter 7,500 kalibrerade år BP sker det en tydlig oceanografisk förändring. Borrkärnan (M23258-2) från havet söder om Svalbard uppvisar inte några av de mönster som de två mer sydligt belägna kärnorna gör. Detta kan bero på att sediment från kontinentalbranten har rörts upp under kraftiga vinterstormar och transporterats ner mot oceanbotten. Undersökningarna genomförda i denna studie visar att hysteresismätningar även ger en indikation av tidigare intensitet av bottenströmmar i Nordatlanten och Norska havet under Holocen.

**Nyckelord**: Magnetisk kornstorlek, magnetiska hysteresis-lopar, Reykjanesryggen, Vøringplatån, Nordatlanten, Norska havet, djuphavsströmmar, Holocen.

# 1 Introduction

Geological studies carried out during the last century have shown that the Holocene has not been a climatically stable epoch (e.g. Bond *et al.* 1997). Classic palaeoecological studies of terrestrial deposits in Scandinavia and North America pointed toward a variable climate (Denton and Karlén 1973). Based on radiocarbon chronology during the Holocene Denton and Karlén found that mountain glaciers advanced synchronously in North America and Europe.

Despite pioneer studies of terrestrial sites in the northern hemisphere, which indicated a climatically variable Holocene (at least at the regional scale) multi-proxy climate data sets extracted from the Greenland ice-cores in the late 20$^{th}$ century have instead been adopted as global "benchmarks", particularly by marine geologists. A climatically stable Holocene was initially inferred from multi-proxy records derived from the GRIP and GISP2 ice cores, as these records were not interpreted to contain any significant fluctuations during the Holocene (Larsen *et al.* 1995). These data sets, such as the $\Delta^{18}O$ derived reconstruction of temperature, were first seen from the perspective of the greater amplitude shifts in climate that occurred during the last glacial cycle, and only recently has the Holocene part of the cryospheric record been considered in detail (Johnsen *et al.* 2001). On the other hand, comparisons between the ice core records and other proxy data from the Atlantic Ocean have shown that neither the Eemian nor the Holocene have been climatically stable (Larsen *et al.* 1995). Since these more subtle but significant variations in Holocene climate were revealed considerable effort has been put into collecting high resolution data from the North Atlantic, partly due to its near proximity to Greenland, and partly due to the need to reconstruct the variability in thermohaline circulation (THC) that may be initiated at high northern latitudes and which affects the global climate system.

Variations in atmospheric circulation over the North Atlantic are known to affect the North Atlantic current (NAC) (Hurrell *et al.* 2001) and the surface wind pattern over the Atlantic can affect the surface current flow direction. Today, the warm NAC that leaves the Mexican Gulf has high salinity (36–37 ‰) due to evaporation. When this high salinity surface current reaches the North Atlantic and the Norwegian Sea it cools down and releases large amounts of heat and moisture to the atmosphere. Westwards moving weather systems fuelled by this heat and moisture transfer promote an oceanic climate in northern Europe that is relatively mild compared to equivalent latitudes on the eastern seaboard of the North American continent. When the NAC is cooled down at high latitudes the cold water sinks because of increased density. If the surface water also freezes the salinity of the surrounding water increases (a process known as brine formation) and this also sinks. The subsurface waters move southwards (as described in more detail later) and contribute to the formation of North Atlantic Deep Water (NADW) and the completion of the THC.

THC is not stable over time. Geological reconstructions show that during the Younger Dryas stadial (YD, 12,700 – 11,550 cal BP) THC became less efficient (Broecker 1998) as large amounts of cold fresh water discharged into the North Atlantic. This influx of fresh water was probably caused by the sudden discharge of large glacial lakes in North America and/or Scandinavia (Colman *et al.* 1994, Jiang *et al.* 1998). Compared to the preceding Alleröd/Bölling interstadial the sea surface temperature (SST) in the North Atlantic fell several degrees during the YD (Fisher *et al.* 2002). At the end of the YD, during the transition into the Holocene interglacial, the Polar-front, Arctic-fronts and the THC moved northward and allowed warm water to reach further north. As a result, SST increased in the Norwegian Sea.

The North Atlantic and Norwegian Sea are now recognized as regions where thermohaline circulation is currently active and where NADW is produced, flowing southwards as part of what is known as the "global thermohaline conveyor" (Broecker 1998). Past changes in the intensity of NADW production or its position of formation are likely to have affected regional climate. The North Atlantic and the surrounding areas are sensitive to climatic changes because the path and intensity of the North Atlantic Current and the formation of North Atlantic Deep Water have altered during the past (Calvo *et al.* 2002). It is believed that such changes have amplified externally forced (e.g. solar) climate changes (Stocker *2000*) in west and north Europe (Hammarlund *et al.* 2003, Magny *et al.* 2003).

Millennial-scale Holocene changes in temperature, deep-water formation and the deposition of ice rafted debris have been inferred from studies of sediment cores recovered from the North Atlantic and Norwegian Sea (Bond *et al.* 1997, Bond *et al.* 2001, Chapman *et al.* 2000,

Andrews *et al.* 2003). Compared to the earlier studies, which used parameters derived from biologic materials (e.g. $\delta^{13}C$, $\delta^{18}O$) and determinations of physical grain size by sieving, this study uses an alternative, mineral magnetic proxy designed to identify changes in the intensity of near bottom currents and the possible discharge of icebergs into the North Atlantic Ocean during the Holocene.

Mineral- (or rock-) magnetic studies have been used to reconstruct climate changes in e.g., Europe, Central Asia and China (Sartori *et al.* 1999). The magnetic properties of lacustrine and marine sediments are often climatically influenced and geological records of magnetic parameters often reflect climate induced variations in sediment provenance and the efficiency of subsequent transport processes (Stoner *et al.* 1996). Examples pertinent to this current study include the identification of ice-rafted-debris (IRD) during Heinrich events (Heinrich 1988, Robinson *et al.* 1995) and the identification of Dansgaard-Oeschger cycles in sediment cores recovered from the North Atlantic (Rasmussen *et al.* 1996a, 1996b, 1997, Moros *et al.* 1997, Snowball & Moros 2003).

Given the successful contribution of mineral magnetic methods to studies of late Pleistocene sediments (marine isotope stages 2 & 3) in the North Atlantic, this study was initiated to explore the possibility of mineral magnetic methods contributing to reconstructions of ocean circulation during the Holocene interstadial. Moros *et al.* (1997) and Snowball & Moros (2003) conducted mineral magnetic investigations on sediments that accumulated on the Reykjanes Ridge during MIS's 2 & 3 and presented the hypothesis that variations in magnetic grain size parameters reflected the efficiency of sorting of allochthonous material by near bottom currents. Simply stated, stronger palaeo-currents were reflected by a larger magnetic grain size and vice versa. This work represents a preliminary application of their hypothesis as extended into the Holocene and forms part of a much larger multidisciplinary collaborative study of three sediment cores recovered from the North Atlantic and Norwegian Sea. Mineral magnetic measurements are rapid, sensitive (parts per million are easily detected) and non-destructive, which normally allows for subsequent, destructive, analyses to be undertaken on the magnetic sub-samples.

The magnetic hysteresis properties of bulk sediment samples taken from three high-resolution cores in the North Atlantic and the Norwegian Sea form the backbone of this project. Initial questions to be answered by this study were: is it may be possible to determine the magnetic grain size and are there distinct stratigraphic changes in individual Holocene sediment sequences? Is it possible to distinguish between different near bottom current regimes and/or identify and trace different sediment sources?

It is known that the most common magnetic mineral in sediment on the floor of the North Atlantic is titanomagnetite (Kissel *et al.* 1999). This titanomagnetite mineral originates primarily from basaltic rock of the Mid-Oceanic Ridge and to a lesser extent from parts of Greenland (Scoresby Sund) and Iceland, from where ii can be eroded and transported by sea surface and sub-surface processes (Rasmussen *et al.* 1996b, Moros *et al.* 1997, Kissel *et al.* 1999, Snowball and Moros 2003).

# 2 Site description and present day oceanography

The study area is the eastern part of the North Atlantic and the Norwegian Sea (Figure 1). The northern part of the Atlantic's surface is influenced by warm currents from the Gulf of Mexico as the North Atlantic current (NAC) that flows northwards around Iceland as the Irminger Current (IC) and between Iceland and the British Isles as a surface current. South of Iceland a gyro of warm water is created. The NAC continues to run parallel to the Norwegian coast and becomes the Norwegian Current (NC). Later the NC becomes the West Spitsbergen Current (WSC) and flows along the western seaboard of Svalbard. On the south side of Svalbard, the East Spitsbergen Current (ESC) from the north interacts with the WSC.

NADW flows southwards through the study area as intermediate depth bottom currents. The path of these intermediate depth currents is partly governed by the oceans bottom topography and the positions of major land masses. Part of the NADW also flows into the Atlantic basin over the Iceland-Scotland ridge and around the Reykjanes ridge, turning northwards for relatively short distance to the west of this ridge and rejoining the EGC. Deep-water formation is believed to occur in the whole study area.

Cold, relatively fresh surface waters from the Arctic Ocean flow southward parallel to the

coast of Greenland and through the Denmark Strait, and known as the East Greenland Current (EGC). This current splits up in two gyros, in the north the Jan Mayen current and in the south, just north of Iceland, the East Icelandic current (EIC). The boundary between the warm surface water from the south (the NAC and its derivatives) and the cold surface water from the north, defines the Arctic front (Calvo *et al.* 2002).

## *2.1 Coring sites*

### 2.1.1 LO09-14

LO09-14 was collected on the Reykjanes ridge in the North Atlantic 59°N, 31°W in a water depth of 1700 m. It consists of a large box core (LBC), a giant gravity core (GGC) and a gravity core (GC). The composite core is 6 m long (Moros *et al.* 2004).

### 2.1.2 MD95-2011

Core MD95-2011 was collected during the IMAGES 101 cruise on the 6th of August 1995. MD95-2011 is a piston core recovered from the eastern Vøring plateau 66°58, 19'N, 07°38, 36'E at a water depth of 1048 m. The sediment sequence is 7.5 m long.

### 2.1.3 M23258-2

The site is situated in the north-eastern Norwegian Sea on the lower Barents continental slope, 75°N, 14°E at a water depth of 1768 m. Core M23248-2 was retrieved during the METEOR cruise on the 7th of February in 1988. It is a composite core consisting of a Kasten core overlapped by a box core. The composite core contains 4.1 m of sediment.

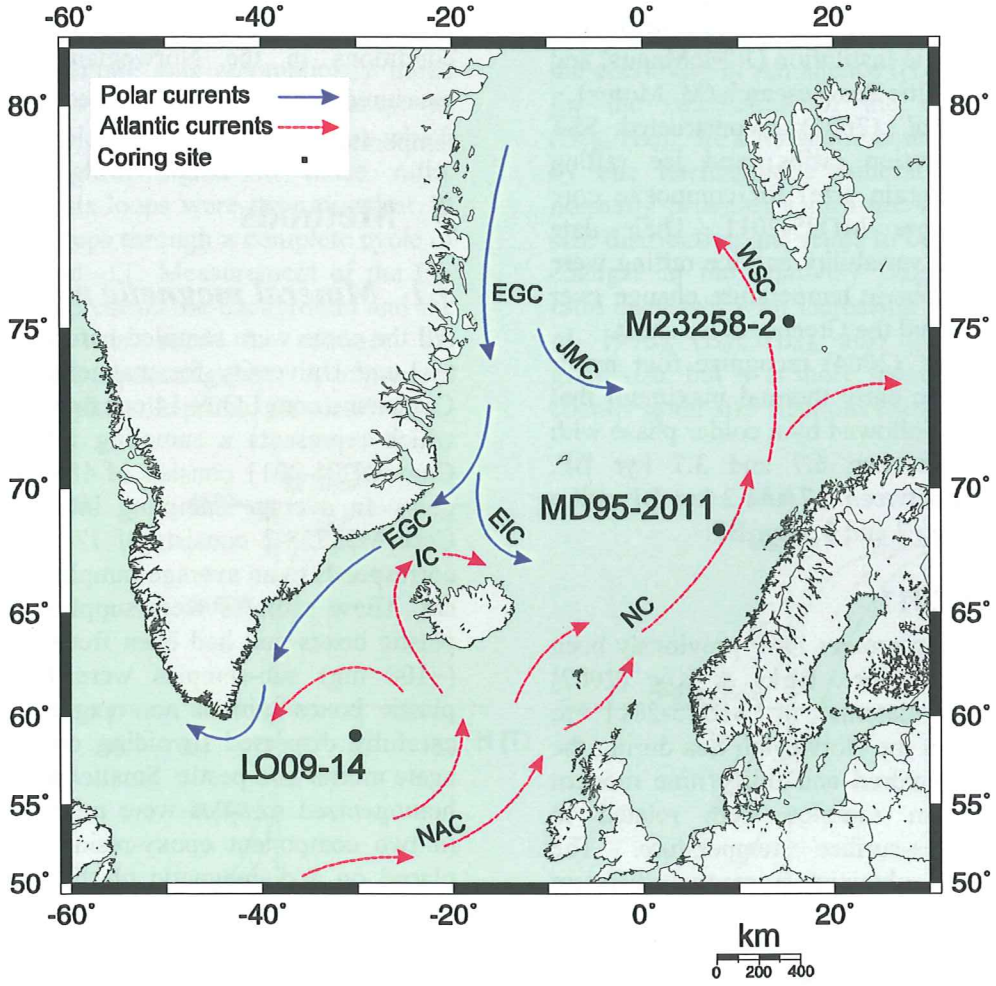


Figure 1. Map of the northern North Atlantic and Norwegian/Greenland Seas. The locations of the cores are marked by solid circles. The modern oceanographic circulation pattern is shown so that warm surface currents are represented by red dotted arrows and cooled surface currents by blue filled arrows. *NAC* North Atlantic current, *IC* Irminger Current and *NC* Norwegian Current are warm surface currents, while the *EGC* East Greenland current, *EIC* East Icelandic current and *JMC* Jan Mayen current are relatively cool surface currents (adapted from Moros *et al.* 2004).

## 2.2 *Previous work on the cores*

This work is part of a larger project. Researchers from the Bjerknes Centre for Climate Research (Bergen, Norway); the Norwegian Polar Institute (Tromsö, Norway), the Woods Hole Oceanographic Institution (USA) and the Baltic Sea Research Institute (Rostock, Germany) are analyzing Holocene SST, ice rafting variability and bottom current strength changes using different proxies on several cores from the North Atlantic. The results in this work may contribute to the reconstruction of relative bottom current speed variability and sediment sources.

### 2.2.1 LO09-14

A variety of biological, physical and chemical analyses are being conducted on this core and the results have yet to be published. The mineral magnetic data set produced during this study contributes to a collaboration between the Woods Hole Oceanographic Institution (J. McManus) and the Institute for Baltic Sea Research (M. Moros).

Moros *et al.* (2004) reconstructed SST (alkenone unsaturation ratios) and ice rafting (mineralogy and grain size) for composite core LO09-14 and core MD95-2011. Their data suggests that SST variability and ice rafting were coupled to atmospheric temperature change over Northern Europe and the Greenland ice sheet.

Moros *et al.* (2004) recognize four major climatic phases, an early thermal maximum that ends 6.7 kyr BP. Followed by a colder phase with increased IRD between 6.7 and 3.7 kyr BP. Unstable phases between 3.7 and 2 kyr BP and a cold phase between 2 and 0.5 kyr BP.

### 2.2.2 MD95-2011

Palaeoceanographic proxies have previously been obtained from this core. Birks & Koç (2002) analysed fossil diatoms in MD95-2011 to reconstruct SST in the Norwegian Sea during the Holocene. One hundred and thirty nine modern sea-surface diatom samples were related to contemporary sea-surface temperature. The transfer functions obtained from two different numerical methods were used to reconstruct SST changes.

Calvo *et al.* (2002) made a study of the $C_{37}$ alkenone distributions in core MD95-2011. The evaluation of $U_{37}^{K}$ and $U_{37}^{K'}$ was possible because of the relatively cool water conditions. They also used measurements of $U_{37}^{K}$ to reconstruct SST's during the Holocene.

Risebrobakken *et al.* (2003) provided evidence for large and small scale climate variations during the Holocene. They used stable oxygen isotopes from both left and right coiling planktonic foraminifera to reconstruct SST using modern analogue transfer functions.

Andersen *et al.* (2004) used the diatom assemblages and reconstructed SST's, which were interpreted in terms of the past distribution of different water masses in the Norwegian Sea.

### 2.2.3 M23258-2

Sarnthein *et al.* (2003) analysed planktonic foraminifera to reconstruct SST at the western continental margin of the Barents Sea. Martrat *et al.* (2003) measured the total organic carbon (TOC) content of the sediment, which they related to planktonic productivity and organic matter preservation. To reconstruct palaeo-climatic conditions in the Norwegian Sea they also measured the $U_{37}^{K}$ index to reconstruct the SST temperature in the area.

# 3 Methods

## 3.1 *Mineral magnetic measurements*

All the cores were sampled before they were sent to Lund University for magnetic measurements. Composite core LO09-14 consists of 419 samples, which represents a sampling interval of 2 cm. Core MD95-2011 consists of 483 samples, which gives an average sampling interval of 1.4 cm. Core M23258-2 consists of 171 samples, which corresponds to an average sampling interval of 2.2 cm. These samples were supplied in 2×2×2 cm plastic boxes and had been freeze-dried. Smaller (~100 mg) sub-samples were taken from the plastic boxes with a non-magnetic spatula and carefully dispersed (avoiding crushing) with an agate mortar and pestle. Smaller amounts of these homogenized samples were mixed with Araldite (a two component epoxy-resin based glue) and placed on a diamagnetic plastic film (~5×5x0.1 mm) before the resin set. The typical weight of the film, glue and sediment for measured sub-samples was approximately 25 mg. The absolute mass of the sediment contained in each resin-based sample is not known, although this is of no significance for the subsequent magnetic hysteresis measurements and the magnetic ratios that form the focus of this study.

The magnetic parameters obtained in this investigation are based on magnetic hysteresis, which can be dependent on ferrimagnetic mineral grain-size. In order to magnetically characterise the samples, magnetic hysteresis loops were measured at ambient room temperature (ca. 20° C). The magnetic hysteresis loops were measured in the Palaeomagnetic and Mineral Magnetic Laboratory (PMML) at the GeoBiosphere Science Centre, Lund University, using a Princeton Measurements Corporation *Alternating Gradient Magnetometer* (PMC AGM M2900-2). A P1-phenolic probe was used for all measurements. The AGM was calibrated using a nickel foil standard (with a room temperature saturation magnetization of $478 \times 10^{-12}$ $Am^2$). The diamagnetic contribution of the P1-probe was measured and subsequently subtracted from the hysteresis loops obtained for each sample. The tip of the probe was initially cleaned by suspension in 10% HCl within an ultrasonic bath for c. 10 minutes, and then washed with alcohol.

Each sub-sample was automatically tuned to find the optimum resonance frequency (as detected by the piezometer in the probe) which provides the highest signal to noise ratio. Magnetic hysteresis loops were determined at 10 milliTesla (mT) steps through a complete cycle of between +1 T and -1T. Measurement of the P1-phenolic probe represents the background and the PMC software was used to subtract the diamagnetic and paramagnetic components residing in the P1-phenolic probe, the plastic film, the resin and the bulk sediment. Finally, the remanence of each sample was measured after application of successive negative steps of 10 mT to a maximum negative field of -100 mT.

Saturation magnetisation ($M_s$) is the highest possible magnetisation that can be induced in a substance at a given temperature (note that pure magnetite saturates at c. 100 mT). Saturation remanence ($M_{rs}$) is the magnetization that remains after the saturating field is removed. Coercive force $(B_0)_c$ is the magnetic force required to return the saturation magnetization to zero. Coercivity of remanence $(B_0)_{cr}$ is the negative field required to return a positive saturation remanence magnetization to zero - see Figure 2 (Stoner *et al.* 1996).

The magnetic hysteresis loop enables the calculation of the ratio between saturation remanent magnetization ($M_{rs}$) and saturation magnetization ($M_s$) - $M_{rs}/M_s$. The hysteresis loop also provides the coercive force ($(B_0)_c$). The negative fields applied to the positive $M_{rs}$ provide the coercivity of remanence ($(B_0)_{cr}$), which allows for the calculation of the coercivity ratio - $(B_0)_{cr}/(B_0)_c$. In a magnetic assemblage dominated by one ferrimagnetic mineral the $M_{rs}/M_s$ ratio normally provides a measure of magnetic grain-size distribution and tends to be more sensitive to changes in the relatively fine fractions. $M_{rs}/M_s$ ratio decreases with increasing grain size (Vlag *et al.* 1996). $(B_0)_{cr}/(B_0)_c$ also gives the magnetic grain-size, but it is more sensitive to changes in coarser grain-size fractions (Stoner *et al.* 1996).

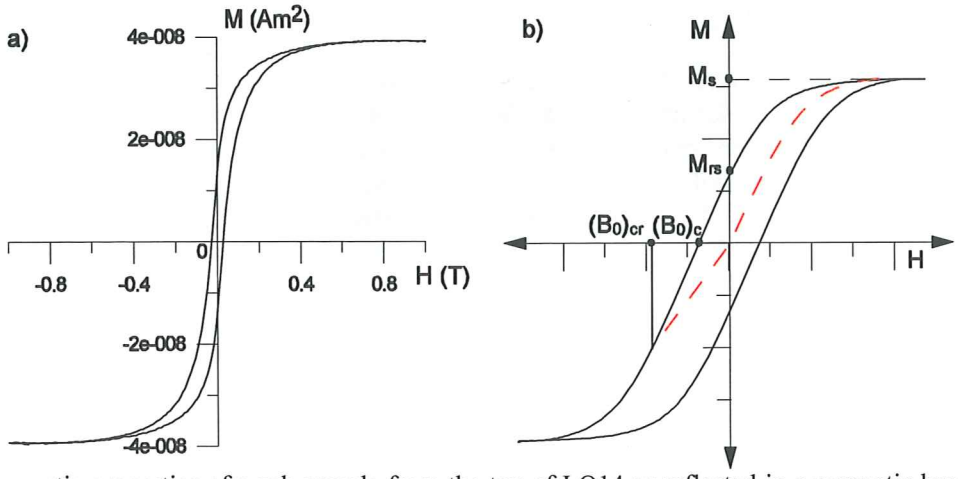


Figure 2. a) The magnetic properties of a sub-sample from the top of LO14 as reflected in a magnetic hysteresis loop. The loop has a wider span between the end points of the open parts than it has in the middle. The loop shape is called "wasp-waisted", which is caused by a bimodal mixture of magnetic grains with different coercive forces. b) Magnetic hysteresis loops have several key positions, which are shown in the idealised loop. The labelled points in the Figure are explained in the text. Coercive force $(B_0)_c$ shows the magnetic "hardness" of the mineral. Coercivity of remanence $(B_0)_{cr}$ is a quantitative measure of the negative field required to reduce the sample to zero remanence after the removal of the positive field.

## 3.2 *Chronology*

Age-models have been constructed by linear interpolation between radiocarbon dated levels after calibration to calendar years. The correction for the marine reservoir effect was assumed to be 400 years for MD95-2011 and M23258-2 (Birks & Koç 2002, Andersen *et al.* 2004, Calvo *et al.* 2002, Risebrobakken *et al.* 2003, Martrat *et al.* 2003, Sarnthein *et al.* 2003). All ages subsequently referred to in this study are in calibrated calendar years BP before 1950 (cal BP) if not otherwise stated.

### 3.2.1 LO09-14

The age model has been published in Moros *et al.* (2004). The overlap between the giant gravity core and the gravity core is based on the correlation of distinct features in magnetic susceptibility, alkenone derived SST and 34 calibrated AMS $^{14}$C dates. The composite core is 6 m and spans from 11366 to 310 cal BP. The $^{14}$C age were calibrated to calendar age by OxCal programme v3.8 (Moros *et al.* 2004).
Time-depth models for cores LO09-14 GC and GGC are based on polynomial fits with the equations (1) and (2). Where X= depth and Y = the determined age

Age equation for core LO09-14 GC
$Y=4221+*33{,}95*X-0{,}085*X^2+9{,}61E-5*X^3$ (1)
Coefficient of determination, $R^2=0.985$

Age equation for core LO09-14 GGC
$Y=2474-2{,}9*X+0{,}0222*X^2+0{,}00084*X^3-2{,}31E-6*X^4$ (2)
Coefficient of determination, $R^2=0.987$.

The composite sequence covers the last 11,000 years. The average sediment accumulation rate is 19 cm/kyr. The composite core consists of a box core LO09-14 GC and two gravity cores LO09-14 GGC and LO09-14 LBC with a total length of 6 m.

### 3.2.2 MD95-2011

The radiocarbon ages for core MD95-2011 were obtained from twelve AMS-$^{14}$C measurements on shells of *Neoglobigerina pachyderma*. The presence of the Vedde ash at a depth of 709.5 cm provides additional time control and this ash has been assigned an age of 11,980 cal BP (derived from the GRIP ice core). The boundary between the Pleistocene and the Holocene (692.5 cm) is assumed to be 11,550 cal BP and has been placed in the middle of the SST rise (Birks & Koç 2002). The AMS $^{14}$C dates are corrected for a marine reservoir effect of 400 calendar years. Calib 4.3 was used to convert the ages to calendar years. The core covers the last 13,805 years. The average sedimentation rate is 5.6 cm per 100 yr (Risenbrobakken *et al* 2003). Age models for MD95-2011 can be found in Birks *et al.* (2002), Andersen *et al.* (2004), Calvo *et al.* (2002) and Risebrobakken *et al.* (2003).

### 3.2.3 M23258-2

The core M23258-2 is dated by 15 AMS-$^{14}$C dates. The AMS-$^{14}$C dates were corrected by a marine reservoir effect of 400 years. Dates at 249 and 250 cm were, however, corrected for a reservoir effect of 900 years because of decreasing ocean mixing of $^{14}$C during the Younger Dryas (Sarnthein *et al.* 2003). Age models for M23258-2 can be found in Martrat *et al.* (2003) and Sarnthein *et al.* (2003). These cores have been dated by AMS-$^{14}$C and tephrochonology.

The Younger Dryas – Holocene boundary was assigned to 320 cm in the core by correlation of the $\delta^{18}$O analyses of N. pachyderma to the $\delta^{18}$O record of the GISP2 ice core. Martrat *et al.* (2003) correlated the $\delta^{18}$O profile of M23258-2 to Termination 1a when the highest values of TOC (Total Organic Carbon) occurs in the core, which is related to the retreat of the Barents Sea ice at 15,000 cal BP. The sedimentation rate for the Holocene has been estimated to 15 cm/kyr from the age model (Sarnthein *et al.* 2003, Martrat *et al.* 2003). The sedimentation rate gradually decreases from >100 cm/kyr during the Early Holocene to 15 cm/kyr in the middle and late Holocene (Sarnthein *et al.* 2003).

# 4 Results

Table 1. The range of values obtained from the core analyses and age modelling, and number of samples measured for magnetic hysteresis properties.

| Core | $(B_0)_c$ (mT) | $(B_0)_{cr}$ (mT) | $(B_0)_{cr}/(B_0)_c$ | $M_{rs}/M_s$ | Depth cm | Age range cal BP | Sample number (n) |
|---|---|---|---|---|---|---|---|
| LO09-14 GGC | 12–32 | 30–70 | 2–3 | 0.2–0.4 | 2–271.5 | 2441–7801 | 119 |
| LO09-14 GC | 12–32 | 30–70 | 2–3 | 0.2–0.4 | 133.5–589 | 4338–11265 | 182 |
| DS-2P | 8–24 | 40–56 | 2–5 | 0.12–32 | 1–142.5 | N/A | 64 |
| DS-2T | 8–24 | 36–52 | 2–4 | 0–0.3 | 1.5–75 | N/A | 34 |
| LO09-14 LBC | 19.9–21.6 | 44–48 | 2.16–2.32 | 0.26–0.3 | 1–43 | 310–1112 | 20 |
| MD95-2011 | 12–22 | 32–48 | 2–3.2 | 0.12–0.32 | 90–745 | 548–13805 | 483 |
| M23258-2 | 8–24 | 25–50 | 1.6–4 | 0.12–0.32 | 26–405.5 | 698–13957 | 171 |

The magnetic hysteresis properties of the cores and the age ranges of the different cores are summarised in table 1.

## *4.1 Magnetic hysteresis ratios*

The magnetic properties of the sub-samples taken from each core are plotted in a so-called "Day plot" (Day *et al.*, 1977). This plot was based on the magnetic hysteresis measurements of natural titanomagnetite samples of known physical grain-size distribution and shows how magnetic hysteresis measurements can produce a magnetic grain-size framework.

The sub-samples from site LO09-14 are plotted in Figure 3a. These samples lie within the pseudo-single domain area (grain-size of 2–63 μm), except for one sub-sample from core DS-2T that has plotted in superparamagnetic grain-size region (grain-size of 0.001–0.01 μm) (Thompson and Oldfield 1986). DS-2T is one of the three top cores from LO09-14.

The magnetic properties of sub-samples from core LO09-14GGC differ significantly from the other cores recovered at the LO09-14 site. Most sub-samples plot within a $M_{rs}/M_s$ ratio range between 0.2 and 0.32, while the $(B_0)_{cr}/(B_0)_c$ ratio ranges between 2 to 3. However, some sub-samples in core LO09-14GGC plot in a $M_{rs}/M_s$ ratio range between 0.3 and 0.4.

The magnetic properties of sub-samples from core MD95-2011 are also plotted as a Day plot in Figure 3b. All the sub-samples behave as collections of pseudo-single domain grains. $M_{rs}/M_s$ ranges between 0.18 and 0.3, and $(B_0)_{cr}/(B_0)_c$ ranges between 2 and 2.5.

The magnetic properties of sub-samples from core M23258-2 are plotted in Figure 3c. All measured samples plot within the pseudo–single grain size range. $(B_0)_{cr}/(B_0)_c$ lies between 2–3 and the $M_{rs}/M_s$ ratio between0.13–0.3. There are some sub-samples that have plotted in a larger span between and 1.9-3.7 and 0.15–0.25.

The different ratios plotted in Figure 3 are employed to characterise magnetic materials in terms of magnetic domain-state and, therefore, relative grain-size or absolute grain-size if such data are available. Evidence exists to support the assumption that the samples analysed here are dominated by titanomagnetite and that the magnetic grain-size model proposed by Day *et al.* (1977) can be applied to extract physical grain-size.

In Figure 4 all the magnetic ratios are plotted against $(B_0)_{cr}$ to separate the different magnetic components. The samples in LO09-14 has two clear populations, one between $(B_0)_{cr}$ of 40 to 50 mT and one population between 55 and 65 mT. In Figure 4b all the samples from core MD95-2011 plot between 35 and 45 mT and all samples are gathered around a line.

Samples from M23258-2 has plotted similar to MD95-2011, between 35 and 45 mT and are also gathered around a line, -see Figure 4c.

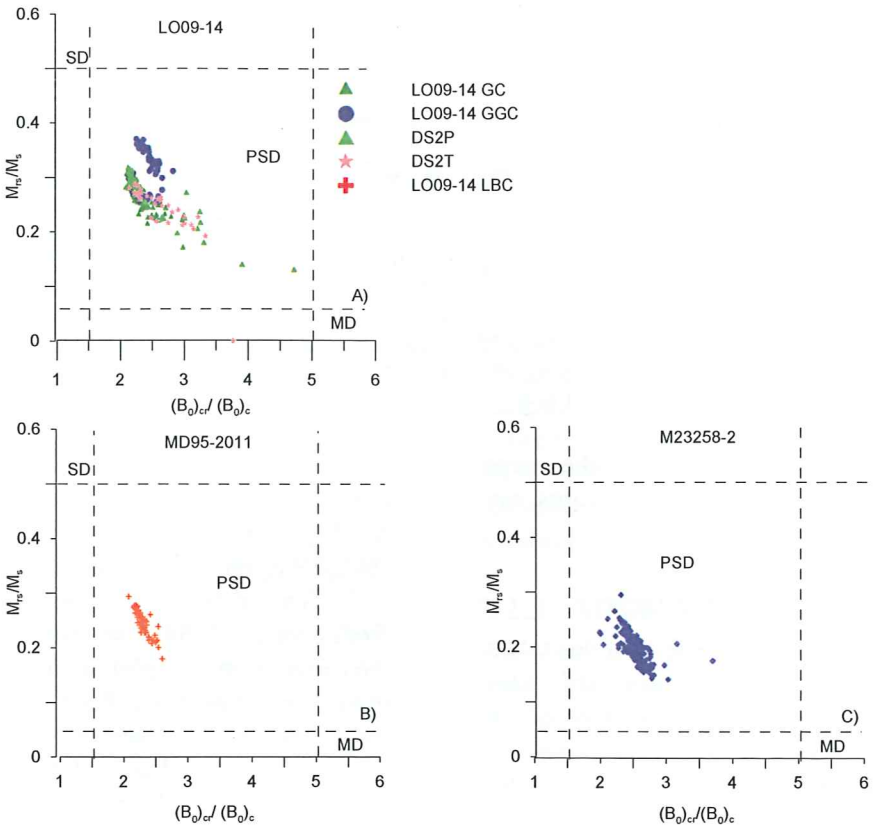


Figure 3. "Day" plots for subsamples from core LO09-14 (a), MD95-2011(b) and M23258-2 (c). All the sub-samples plot in the pseudo-single domain area. Note that a distinct population of samples in LO09-14GGC have $M_{rs}/M_s$ ratios above 0.32, which are not seen elsewhere.

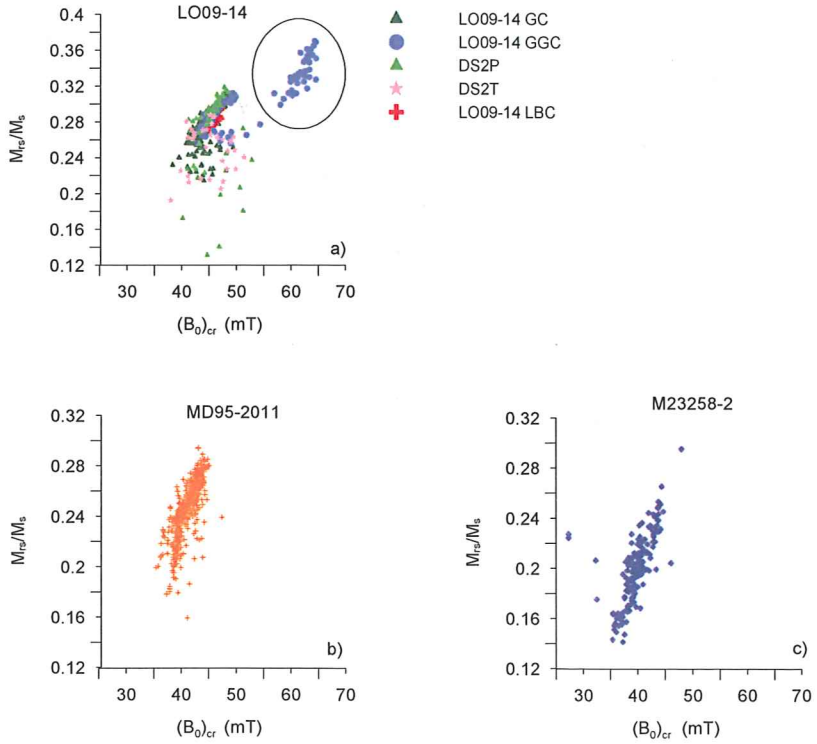


Figure 4. Figure 4a, b and c are plots of $M_{rs}/M_s$ versus $(B_o)_{cr}$. The circle shows the distinct set of samples from LO09-14GGC that have considerably higher coercivity and coercivity of remanence compared to the other samples analysed. In general, there appears to be more variability within the LO09-14 sediment sequence than the other two cores.

## 4.2 *LO09-14*

The graphs in Figure 5 show magnetic hysteresis data from cores DS2P, DS2T and LO09-14LBC. These three top cores taken at the LO09-14 site do not have a composite depth or age-depth model. To avoid misinterpretation these cores have not been superimposed on the others, and have instead been plotted as separate graphs in Figure 5. The depth scale is the same for all graphs, but the values of the magnetic parameters have a different span compared to the - see also table 1.

The top cores show similarities, but they are highly variable between 80 and 20 cm and then all cores becomes relatively stable.

Figure 6 shows all the magnetic data for the composite core consisting of LO09-14GC and LO09-14GGC. The overlap was established through a variety of techniques, which is verified by the good agreement between the two magnetic hysteresis data sets. This correlation (section 3.2.1) requires that 130 cm be added to the depth scale of LO09-14GC.

Figure 6a shows the values of coercive force $(B_0)_c$ versus depth, which has a lower unit of fluctuating values (from 15.4 to 20.5 mT) between 589 cm and 442.5 cm. Between 442.5 and 180.5 cm the values are stable at ca. 19 mT. Above 342 cm, $(B_0)_c$ increases to 23 mT and after 180.5 cm it starts to decrease again. The value keeps decreasing down to 19 mT at 86.5 cm. There is a spike at 116.5 cm that reaches 25.1 mT. After 86.5 cm and all the way to the top $(B_0)_c$ fluctuates.

Figure 6b displays the coercivity of remanence $(B_0)_{cr}$, which is related to $(B_0)_c$ and follows the same trend as $(B_0)_c$. The interval between 589 cm and 497 cm $(B_0)_{cr}$ displays fluctuating values and has a minima of 41.7 mT at 537 cm. Between 497 cm and 264.5 cm the $(B_0)_{cr}$ values are relatively stable at values of ca. 42 mT. Above 264 cm the values increase and reach maximum levels of ca. 50 mT at 214 cm. Values decrease to 44.4 mT at 105.5 cm with a distinct spike at 116.5 cm of 61.8 mT. Values rise towards the top of the core LO09-14 GGC and attain a maximum value of 64.6 mT.

The $(B_0)_{cr}/(B_0)_c$ ratio is shown in Figure 6c. A lowermost segment from 589 to 442.5 cm of core LO09-14 displays values that fluctuate between 2.14 and 3 mT. Between 537 cm to 497 cm the values are relatively stable except for a value of 2.14 at 520.5 cm. Above a depth of 442.5 cm there is a section of stable values, which ends at 128 cm, where the coercivity ratio rises to 2.58 at 79.5 cm. At 116.5 cm there is a spike of 2.45. Above 79.5 cm the ratio decreases up to the top of the core.

Figure 6d shows the $M_{rs}/M_s$ ratio, which is variable from the bottom of the core at 589 up to 438 cm; the ratio ranges between 0.22 and 0.28 in this part. Between 438 and 285.5 cm the magnetisation ratio is relatively stable around 0.26 except for a low value of 0.21 at 338 cm, where the ratio reaches 0.21. Above 285.5 cm the two overlapping core sections do not match perfectly in terms of this magnetic ratio, although they display the same trend of rising $M_{rs}/M_s$ up to 214 cm, above which there is a decrease to 86.5 cm. There is a distinct spike in the ratio of 0.33 at 116.5 cm. Between 86.5 cm and the top of the core LO09-14 GGC there is a rapid rise in the ratio of $M_{rs}/M_s$ to 0.36, with some superimposed variability.

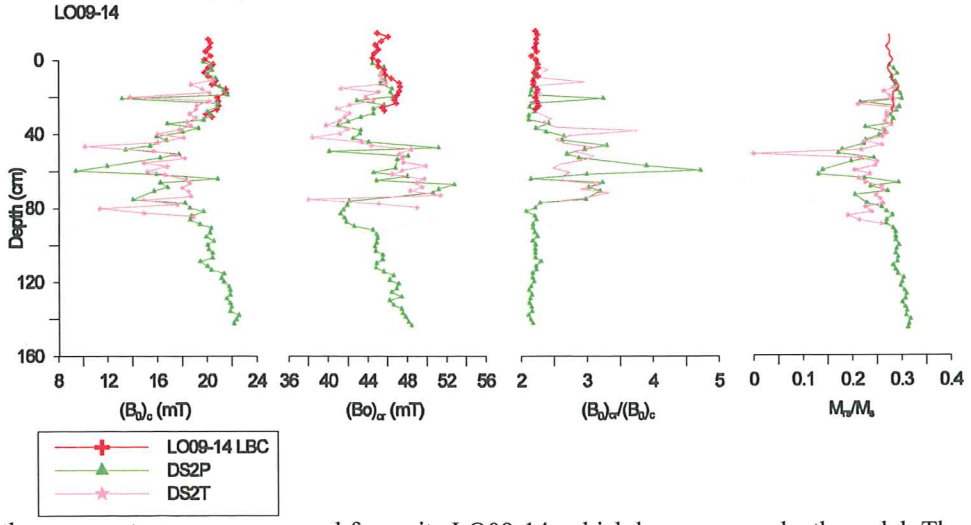


Figure 5. The three upper top cores recovered from site LO09-14, which have no age-depth model. The overlaps see in the figure were established by matching significant features in the magnetic hysteresis data and it must be stressed that these are preliminary correlations.

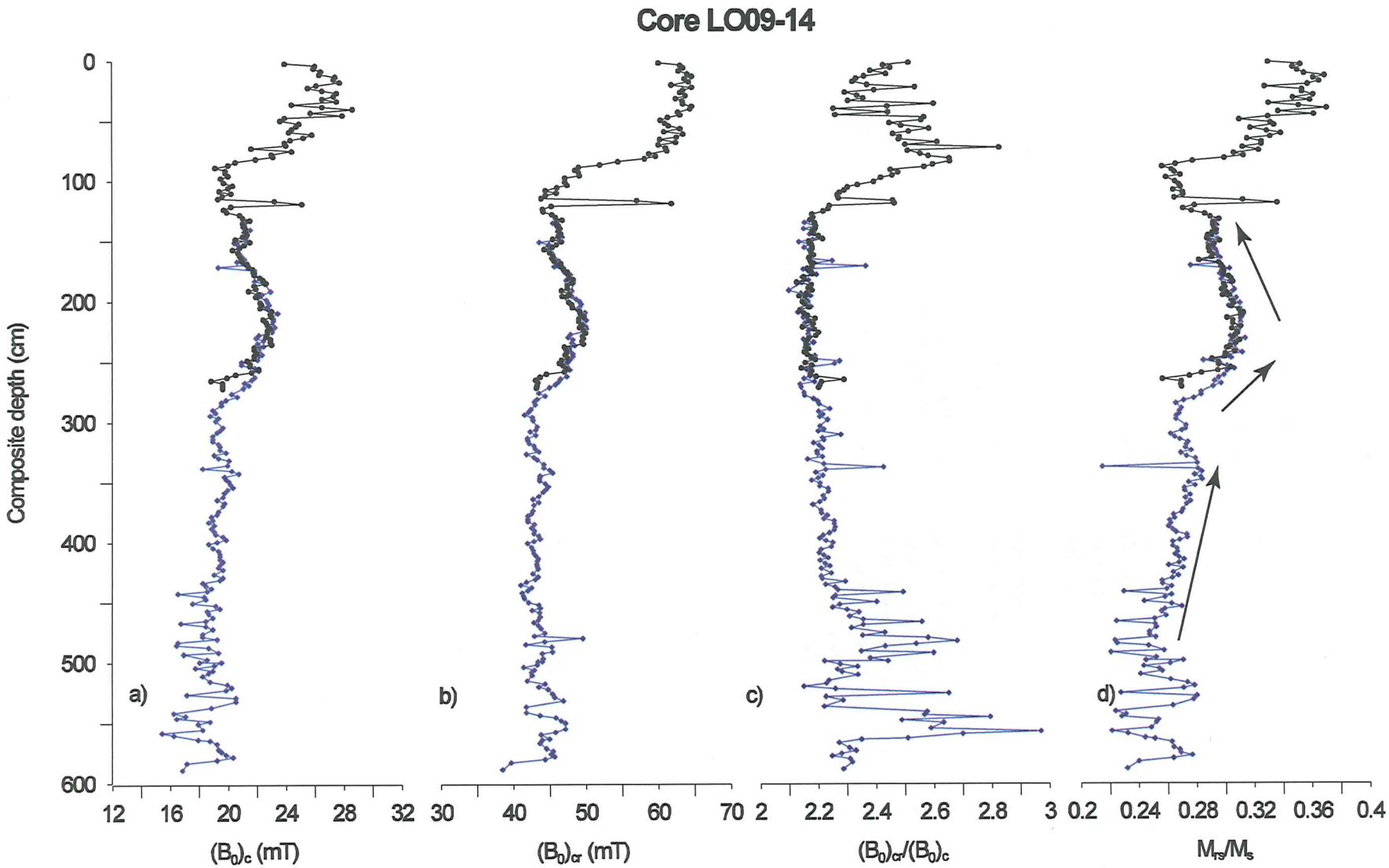


Figure 6. The magnetic hysteresis data for LO09-14 GC and LO09-14 GGC plotted against depth. All curves show the same trend. Notable are the high values in the top of the core and the variable sequence in the bottom of the core. At 300 cm there is an apparent shift to higher values of all parameters and ratios. Note is also the spike at 116.5 cm.

## 4.3 MD95-2011

Magnetic hysteresis data obtained on core MD95-2011 are shown in Figure 7. $(B_0)_c$ and $(B_0)_{cr}$ are shown in Figures 7a and 7b, respectively. The two ratios, $(B_0)_{cr}/(B_0)_c$ and $M_{rs}/M_s$ are shown in Figures 7c and 7d, respectively.

Figure 7a shows that in the bottom of core MD95-2011, from 745 cm to 685 cm $(B_0)_c$ fluctuates between 19.4 and 14.7 mT, but above 685 cm the values are relatively stable. At this depth $(B_0)_c$ increases and reaches 19.1 mT at 645 cm. From 645 cm to 462 cm $(B_0)_c$ decreases. The low value of 14.3 mT at 532 cm is the most prominent feature. There are small variations at 593 cm and 620.5 cm. The values decrease until 462 cm and increase above this level. This trend stops at a depth of 185.5 cm with a value of 20.1 mT. Between 185.5 cm and the top of the core the values of $(B_0)_c$ decrease.

The downcore log of $(B_0)_{cr}$ (Figure 7b) is similar to that of $(B_0)_c$. From the bottom of the core at 745 cm to 645 cm the values fluctuate between 40.3 mT and 35.9 mT. From 645 to 569 cm $(B_0)_{cr}$ decreases to 40.7 mT. Between 620 and 593 cm there is a large fluctuation, which is also represented in the $(B_0)_c$ graph. From 462 cm $(B_0)_{cr}$ values increase to the top of the core.

The $(B_0)_{cr}/(B_0)_c$ ratios are shown in Figure 7c. From the bottom of the core up to 669 cm there is a sequence of fluctuating values. At 669 cm the variability decreases and the values are relatively stable up to 535 cm. There is one high value of 2.5 at 620 cm. Above 535 cm the $(B_0)_{cr}/(B_0)_c$ ratio increases and reaches a maximum of 2.7 at a depth of 430 cm. The general trend between 440 and 326 cm is of declining values. The values between 326 cm and 76 cm are quite constant, with little variability. The ratio attains its lowest value of 2.08 between 278 and 235.5 cm. Above 76 cm the values increase to the highest values of 3.0 in 29.5 cm, although there are fluctuations up to the top of the core.

The $M_{rs}/M_s$ ratio is displayed in Figure 7d. In the lower parts of core MD95-2011 the values are low, down to 0.18 at 685 cm. The values increase above 645 cm and reach stable values at 535 cm. One spike in this sequence occurs at 620 cm with a relatively low value of 0.21. After 535 cm there is a section of highly fluctuating values, above 490 cm the values increase again until 326 cm. The low spike at 392 cm reaches a ratio value of 0.186. The fluctuating period between 326 and 76 cm is varying around a stable mean value of 0.264. Above 76 cm and up to the top of the core, the values are highly variable, reaching a minimum of 0.159.

## 4.4 M23258-2

Figure 8 presents the magnetic data for M23258-2. Between 404.5 and 310.5 cm, a sequence characterised by variability in $(B_0)_c$ culminates in a spike at 17.4 mT. Above the spike at 310 cm the values are increasing between level 297.5 and 253 cm. The sediment between 253 cm and the top of the core M23258-2 is characterized by some variability, although the trend is of increasing values of $(B_0)_c$. Four low spikes are obvious at 197, 161.5, 139 and 45.5 cm with measurements of 12.8, 10.2, 8.77 and 13.7 mT respectively.

Coercivity of remanence $(B_0)_{cr}$ in Figure 8b is similar to the curve of saturation coercivity. The fluctuations in $(B_0)_{cr}$ are less prominent, but they do follow the same trends as $(B_0)_c$. High values are present at the bottom of the core, where they are most variable up to a depth of 353 cm. Above 353 cm there is less variability, although the values indicate an increasing trend. Some low spikes are present at 161.5, 139 and 45.5 cm, which have values of 32.3, 32.5 and 27.3 mT respectively.

The ratio of coercivity $(B_0)_{cr}/(B_0)_c$ in Figure 8c begins with a fluctuating sequence of 94 cm from 404.5 to 310.5 cm. At 310.5 cm the ratio drops to 2.2 and above 300 cm the ratio increases again to 2.8 at 297.5 cm. A variable zone of decreasing ratio is present from 297.5 to 253 cm. Above 253 cm the ratio stabilises at values of ca. 2.5, but still with some fluctuations at least in the bottom of this part of the sequence. Anomalous values can be seen at 197, 161.5, 139 and 45.5 cm. The three lowermost anomalies have high ratios 2.97, 3.16 and 3.7, while there is a low value of 1.99 at 45.5 cm.

Figure 8d shows the magnetic ratio $M_{rs}/M_s$, which is variable between 404.5 and 253 cm. Between 310.5 and 297.5 cm there is a distinct plateau with high $M_{rs}/M_s$ ratio of 0.22. The next plateau is between 253 and 237 cm with stable values of 0.2, above there is a decrease in the ratio. From 237 cm to the top of the core the ratio is variable and the trend is of increasing magnetic ratio.

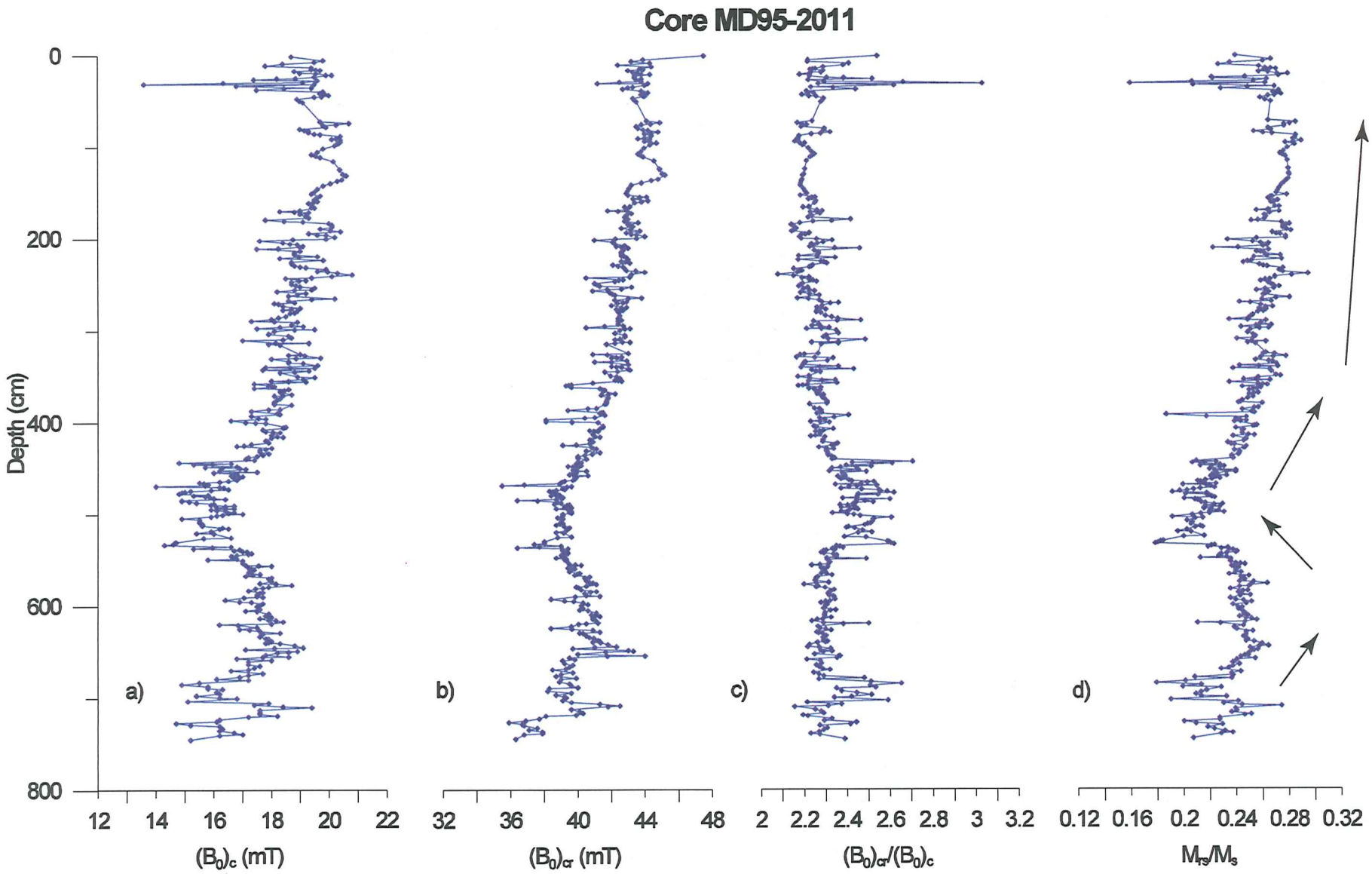


Figure 7. Magnetic hysteresis data for core MD95-2011. All the graphs show similar features. There is variability at the bottom and the top of each graph. Between 550 and 450 cm is a sequence with low magnetic values in graph a) and b). And the magnetic ratio in graphs c) and d) shows similar features.

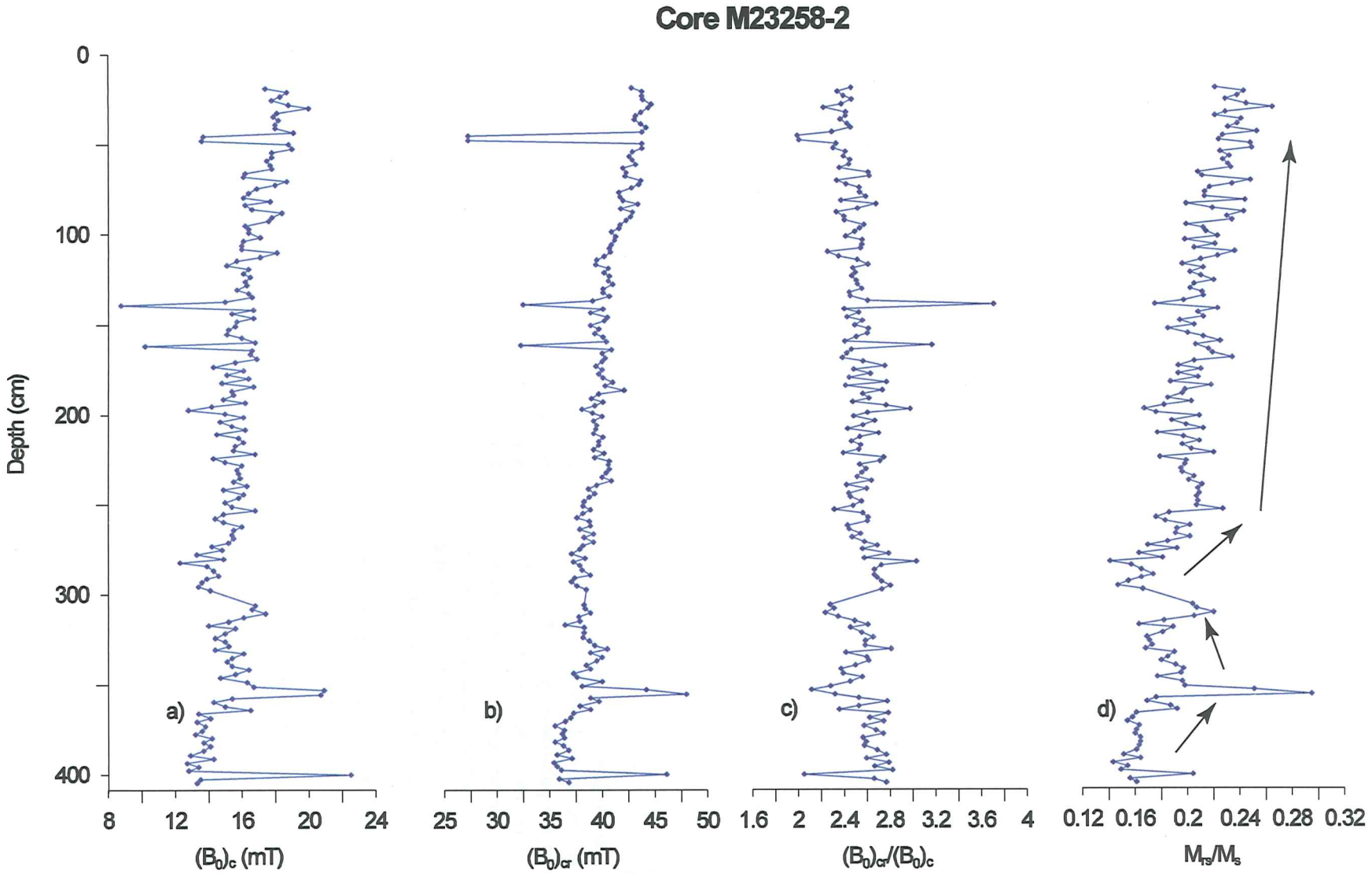


Figure 8. Magnetic hysteresis data for core M23258-2. (a) Coercive force $(B_0)_c$ begins with a variable zone between 250 and 400 cm, which contains three plateaus with low values. (b) Coercivity of remanence $(B_0)_{cr}$ is similar to (a) but with smaller variations. (c) Coercivity ratio shows high spikes but is relatively constant with decreasing values. (d) Magnetic ratio shows low values in the bottom of the core which decreases above 250 cm. The zone between 300 and 250 cm with low values is notable. a, b and d display an increasing long term trend.

# 5 Interpretation

## 5.1 *Comments on the chronological control*

Site LO09-14: Two cores analysed at site LO09-14, DS2P and DS2T have not yet been dated. These cores are expected to fill the chronological gap that exists between 2,000 cal BP (the top of core LO09-14GGC) and 1,112 cal BP (the bottom of LO09-14LBC). Until these dates are available, it is not possible to discuss the temporal development of the mineral magnetic stratigraphy of these cores.

LO09-14 GGC is believed to overlap with LO09-14 GC, which is supported by the good agreement between the overlapping magnetic data. It should be noted that core LO09-14 GGC has greater penetration depth and the upper sediment in this core may have been compacted to a greater extent. It is also possible that the core site position moves between individual corings because the water in the ocean is dynamic. The research vessels use dynamic stabilizing systems to compensate for vessel movement during coring to minimize the errors. However, there is no guarantee that each core taken at an individual site will recover sediment sequences with identical depth/age relationships.

Site MD95-2011: The depth/age relation is based on a linear interpolation between dated levels and ranges between 13,805 and 548 cal BP. According to the published age-depth model the last 548 years were not recovered. This implies that the sediment surface is not modern, and that sediment was lost during core recovery or that no sediment has accumulated at this site during the last c. 550 years. (Risenbrobakken *et al* 2003)

Site M23258-2: This is near the Barents shelf. Calibrated ages are reversed in the deeper parts and the age/depth relation is not linear (Sarnthein *et al.* 2003). High-density turbidity-currents have been detected in the core, so the injection of reworked organic matter is possible (Sarnthein *et al.* 2003). This reworked material might be responsible for AMS-14C dates that do not follow a trend of increasing age with increasing depth (Sarnthein *et al.* 2003). The published age model spans between 13,957 and 698 cal BP.

At the bottom of core MD95-2011 and M23258-2 a much larger marine reservoir age has been assumed. The assumed marine reservoir age is at 800 to 1,000 years around 12,000 cal BP (Björck *et al.* 2003). The reservoir effect is influenced by variations in $^{14}C$ production and the carbon cycle, both of which are variable over time (Laj *et al.* 2002).

## 5.2 *Magnetic grain size behaviour*

Various studies have shown that the mineral magnetic assemblage of late Quaternary sediments recovered from the North Atlantic is dominated by titanomagnetite (Moros *et al.* 1997, Kissel *et al.* 1999, Watkins *et al.* 2003, Snowball and Moros 2003). This titanium poor magnetite originates from quickly cooled basaltic magma, mainly as a detrital product from Iceland and the Mid-Oceanic Ridge that extends south of Iceland and Iceland-Faroe Ridge to the Faroe Islands.

According to the Day plots in Figures 3 and the plots in Figure 4 the measured samples have quite similar magnetic hysteresis properties. The values of the magnetic hysteresis ratios ($M_{rs}/M_s$ = 0.2–0.3 and $(B_0)_{cr}/(B_0)_c$ = 2–3) show that the ferrimagnetic properties are similar to those obtained from previous studies of Quaternary sediments recovered from this region (Snowball and Moros 2003, Watkins *et al.* 2003).

There are some sub-samples in core LO09-14 that can be considered as outliers. In cores DS-2D and DS-2T there are also some samples that appear as outliers, plotting outside the limits of the main population. Most of the samples from core LO09-14 GGC have plotted in the span between 0.3–0.2 $M_{rs}/M_s$ and 2–2.75 $(B_0)_{cr}/(B_0)_c$, and the top of the core is concentrated between 0.3–0.4 $M_{rs}/M_s$ and 2–2.75 $(B_0)_{cr}/(B_0)_c$ (Figure 3a). The high values of coercive force *and* the wasp-waisted hysteresis loops in core LO09-14 GGC indicate that at least one additional magnetic mineral with a high coercive force influences the magnetic hysteresis data. This invalidates the interpretation of the data in terms of the grain size variability of a single component, thought to be titanomagnetite (see Figure 4a). This apparent mixture of magnetic minerals sediments younger than 3000 cal BP at the LO09-14 site suggests that the concentration of the additional magnetic mineral is increasing or that the concentration of titanium poor magnetite has decreased. Additional concentration dependent measurements are necessary to solve this conundrum. In any case, these changes in the magnetic properties occurred between 3,000–2,000 cal BP (Figure 9a).

Cores DS-2P and DS-2T have also plotted outside the range of values displayed by the main

population of samples from this site. These samples have different magnetic properties and are "wasp-waisted," which indicates that the magnetic properties are affected by at least one other magnetic mineral, or that there is a bimodal grain size distribution. The data show that the relative proportions of the two magnetic minerals in the assemblage have changed, most likely due to a change in sediment provenance, rather than a change in near bottom current speed, which would simply alter the magnetic grain size (see also Figure 4a).

The oldest section of core LO09-14, between 11,000 and 9,500 cal BP is characterised by fluctuating values. The relatively large magnetic grain size indicates some influence of IRD, which probably represents the lingering effect of Northern Hemisphere deglaciation. Therefore, it is difficult to determine current flow speeds from the sediments in this age range.

The magnetic grain size remained relatively large until ca. 8,000 cal BP, when a trend of coarsening began, which lasted until 3,000 cal BP. The spike at 3,500 cal years BP with finer magnetic grains is visible in both graphs from LO09-14.

The oldest section of the core MD95-2011 (13,800-10,500 cal BP) is characterised by fluctuating magnetic properties (Figure 9b). These fluctuations may represent the sporadic influence of coarse IRD on the magnetic properties. However, a relatively long period of coarse magnetic grains size is identified between 12,000 and 11,500 cal BP, which most likely indicates increased current flow at this time (the hysteresis loops show no sign of a bimodal grain size distribution, or a multi-component magnetic mineral assemblage). The period between 11,500 and 8,000 cal BP is characterised by a finer magnetic grain size. A period of distinctly coarser magnetic grain size can be seen between 7,500 and 6,500 cal BP. After 6,500 cal BP the magnetic grain size decreases and this trend continues to 1,500 cal BP. The top of the core is unstable with the largest magnetic grain sizes occurring at 500 cal BP.

The Holocene magnetic grain size- trends seen in Core M23258-2 (Figure 9c) are weak. Magnetic grain size is highly variable in the oldest section of the core, between 14,000 and 13,500 cal BP. After a period of relative stability between 13,500 and 12,500 cal BP there is a period of distinctly fine magnetic grain size between 12,500 and 12,000 cal BP. With the exception of the very oldest material, the coarsest magnetic grains accumulated between 11,800 and 10,000 cal BP. From this time forwards there is a gradual fining of magnetic grain sizes.

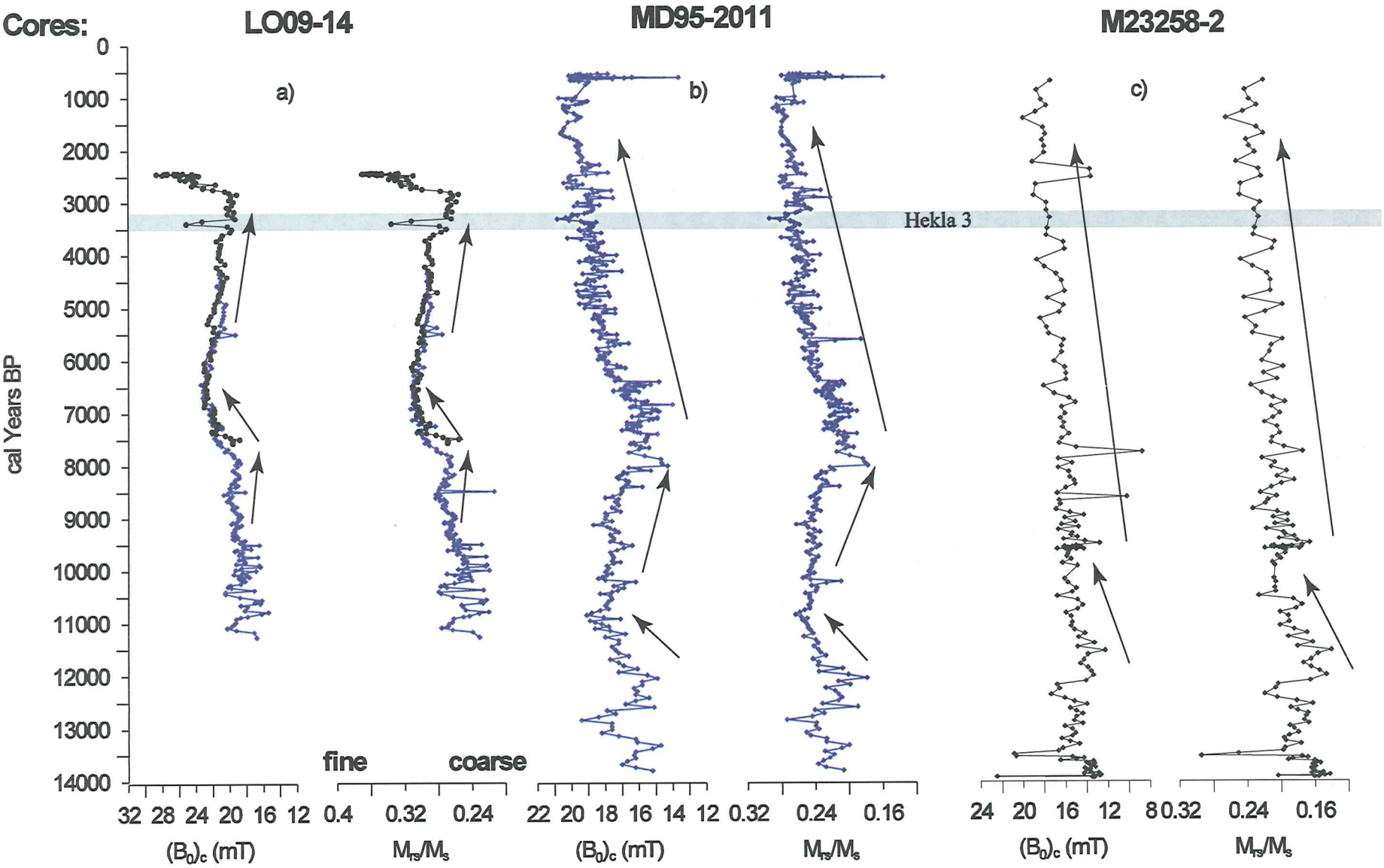


Figure 9. A summary figure of the characteristic magnetic data for the three cores studied plotted against their individual timescales. See text for a general description of the main trends and their interpretation. Note also the possible chronological position of the Hekla 3 tephra, which might have been identified by the magnetic data.

# 6 Discussion

One distinct advantage of magnetic hysteresis measurements made with an AGM is that only relatively small amounts of valuable material are required for analysis. Conversely, questions may be raised regarding sub-sample representation of the bulk sediment. In addition, although there is a well established magnetic grain size framework established for pure magnetite and titanomagnetites of known composition, it is not well established how well these frameworks apply to less well characterised natural assemblages. These mineral magnetic shortfalls can be addressed through comparative analyses.

In the North Atlantic the hysteresis measurements represent the bulk sediment fairly well because of their relatively fine grain size distribution. Relatively coarse grained IRD in the North Atlantic is reflected in XRD as peaks in quartz and the quartz/plagioclase ratio (Snowball and Moros 2003). Larger fragments of biological remains will not contribute to the magnetic hysteresis ratios.

It is difficult to transform the magnetic hysteresis properties to physical grain sizes due to the potential for derived magnetic grain size to vary according to chemical composition. For example, the addition of titanium as an impurity to a single grain of magnetite of a specific physical grain size will cause the same particle to magnetically behave as smaller grain (Vlag *et al.* 1996). Changing sources could, therefore, lead to changing magnetic grain size, even if the physical grain size distribution remains constant. Thus, the sources of magnetite in the sediments must be discussed.

## *6.1 Sources of titanomagnetite*

Watkins *et al.* (2003) and Pirrung *et al* (2002) investigated the sources of magnetic minerals in surface sediments recovered from the North Atlantic Ocean. They discuss the transport of magnetic minerals in the Atlantic Ocean and determined that in the North Atlantic and the Norwegian Sea the main factors affecting the transport of magnetic minerals are:

- Melt out from calving icebergs (IRD)
- Aeolian transport
- Sorting and redistribution of sediment by bottom currents

According to Watkins *et al.* (2003) the surface sediments in the study area in the present day North Atlantic are characterised by relatively coarse ferrimagnetic minerals that (i) originated from the mid-oceanic ridges or (ii) were deposited as volcanic ashes. Surface sediments in the Norwegian Sea are characterised by relatively low inputs of haematite-bearing dust and IRD, and some bacterial magnetite (Watkins *et al.* 2003) so even there the magnetic properties are also dominated by titanomagnetite. At the same time, one must consider that surface sediments are not necessarily modern, unless they are dated to be so (for example, if they contain post-atomic bomb radiocarbon).

The magnetic hysteresis data indicate that magnetic minerals in the lower parts of core LO09-14 originates from basaltic provinces. According to the Day plot in Figure 3a the magnetic mineral would be interpreted as titanomagnetite (Thompson and Oldfield 1986, Snowball & Moros. 2003). In the Norwegian Sea the main magnetic mineral is also titanomagnetite, at least according to the Day plots in Figures 3b and 3c from core MD95-2011 and M23258-2. There is no evidence of a significant bacterial magnetite contribution, in agreement with Watkins *et al.* (2003). The settings during the early and middle Holocene, however, may have been different compared to today.

The transport of magnetic minerals to the sites of investigation is mainly long distance. An alternative to aeolian and bottom current transport of basaltic magnetite is ice rafting, particularly from Scoresby Sund (Greenland) and Iceland. Pirrung *et al.* (2002) argue that when the coast of Greenland and the Norwegian Sea were ice covered during MIS 3, calving icebergs from Scoresby Sund could not reach the open water of the North Atlantic south of Iceland. During relatively warmer periods, when sea ice cover was less extensive, icebergs could be transported by the EGC through the Denmark Strait into the North Atlantic. These icebergs were subsequently transported by anticlockwise surface gyros into the Norwegian Sea. Thus, Pirrung *et al.* (2002) argue that records of increased IRD deposition in these regions correspond to warmer climatic periods in the North Atlantic. In contrast, the Heinrich IRD layers (Heinrich 1988) mainly consist of quartz and non-basaltic feldspars (Moros *et al.* 2002). This could indicate different

source areas and different transport means for IRD and sediments during warm periods.

During the Holocene interglacial the oceanographic settings are quite different to glacials and stadials. The sea ice cover is less widespread in the North Atlantic and the Norwegian Sea and there are no such barriers to prevent icebergs reaching the North Atlantic.

## 6.2 *Magnetic grain size: a proxy of current flow or sediment source?*

The previous interpretations and discussion suggest that the variations seen in the investigated cores are due to magnetic grain size variation (apart from the upper sections of LO09-14 GGC in the composite core LO09-14).

Snowball and Moros (2003) showed that on the Reykjanes Ridge the magnetic grain-size data provide a clear record of grain-size variability in the silt fraction during MIS's 2 and 3, where Dansgaard-Oeschger cycles 3 to 13 were characterised by a steadily increasing grain size and hence current flow. Rapid decreases in grain size (and hence current flow) were coupled to IRD peaks (as determined by XRD). However, the magnetic grain size data were clearly influenced by IRD during the LGM, and by the presence of Ash zone II at c. 52 kyr BP. This study indicates that mineral magnetic studies of high-resolution temporal change in interglacials are probably more complex. The sediment that has accumulated at site LO09-14 since c. 3,000 cal BP has distinctly different magnetic properties as a result of a multi-component magnetic assemblage. Further work is required to determine the sources of these components.

A grain size range between 10 – 63 μm includes the "sortable silt" fraction, which has been advocated as the most suitable fraction for bottom current speed reconstruction (McCave *et al.* 1995). Larger, lithogenic components > 63 μm are usually either IRD or volcanic in origin (McCave *et al.* 1995). Deep sea currents are rarely able to transport quartz grains larger than 63 μm. Grains of titanomagnetite are denser (*c.* density = 5 g/cm3) than grains of silicate minerals (density = 2.67 g/cm3), so grains of comparable size may respond differently to the same current flow intensity.

Grain sizes coarser than 10 μm behave like single particles in suspension and are size-sorted according to shear stresses (McCave *et al.* 1995). Grains smaller than 10 μm become cohesive and the van der Waals force becomes important in particle adhesion (McCave *et al.* 1995). These smaller cohesive particles can aggregate and be sorted as larger particles when influenced by currents. When ferrimagnetic grains lie closely packed, magnetostatic interactions can modify their overall magnetic behaviour and tend to lower the coercivity of the bulk sample (Thompson and Oldfield 1986).

Physical grain size data for some parts of core MD95-2011 (between 7,000 and 9,000 cal BP) were published by Risebrobakken *et al.* (2003). They show that 95% of the grains are smaller than 63 μm. Moros *et al.* (2004) have published grain size data for core MD95-2011 which shows that only between 1 and 32 wt % of the grains were larger than 63 μm during the Holocene. The highest value of 32 % (>63 μm) and 5 % > 150 μm is associated with the 8.2 kyr cold event and is believed to represent IRD (Moros *et al.* 2004). The coarsest Holocene magnetic grain sizes were preserved between 9,000 and 6,000 cal BP (Figure 10), which is synchronous with high SST's. Snowball and Moros (2003) argued that titanomagnetite found in the sediment of the North Atlantic could be determined by two factors or a combination of the two; change in the sediment source and variation in transport and deposition mechanisms. The result of this study combined with other proxies provides only one possible mechanism for the variation seen in the magnetic grain-size distribution between 8,000 and 6,000 cal BP in MD95-2011; hydrological sorting. On the other hand, the magnetic properties of many sections of the cores studied indicate the influence of coarse grained IRD, particularly during the Early Holocene. The most recent sediments in MD95-2011 may also contain influential IRD.

## 6.3 *Palaeoceanographic and palaeoclimatic implications*

Bianchi *et al.* (1999) related coarser grain size in the south Iceland basin and faster flowing Iceland – Scotland Overflow Water (ISOW) when the climate in Europe is warmer, and THC was more active. During the early Holocene they saw a different mode with slower ISOW flow during periods with warmer climate in Europe.

Given the incomplete Holocene record at the LO09-14 site and the rather low resolution data set obtained from M23258-2 this section focuses on the data obtained from core MD95-2011. These data can also be compared to reconstructed SST's published by Calvo *et al.*

(2002) and Birks & Koç (2002). These three data sets and the calculated July insolation at 65°N (Berger and Loutre 1991) are shown in Figure 10.

In the early Holocene the SST curves (Figure 10) are significantly different. The SST proxies from Calvo *et al.* (2002) are based on $U_{37}^{K}$ and the proxies from Birks & Koç (2002) are based on diatoms. It is possible that the different proxies represent temperatures in different seasons and/or in different water depths (Moros *et al.* 2004). The diatom based SST reconstruction reflects the short term summer season. The magnetic grain sizes is markedly more similar to the alkenone-based SST reconstruction made by Calvo *et al.* (2002)

The high concentration of course grain sizes from 12,000 to 11,500 cal BP is most likely due to melting ice bergs. Moros *et al.* (2004) show that the bottom part of the core has a high concentration of Q/plag ratio, which indicated high IRD input.

The start of the Holocene, which is seen as a rapid increase in SST of about 4°C is coupled to relatively finer magnetic grain sizes compared to the IRD influenced YD. The lowest magnetic grain size in the Early Holocene occurs at 10,800 cal BP. From the start of the Holocene at 11,500 to 9,500 cal BP the magnetic hysteresis data are still influenced by IRD. When the grain size variation stabilised after 9,500 cal BP, large inputs of IRD to the North Atlantic and the Norwegian Sea become less common.

The rapid rise of SST's over the Vøring plateau at 11,500 cal BP (Figure 10) is followed by a short cooling around 10,000 cal BP (Birks & Koç 2002). The magnetic grain size in core MD95-2011 became finer at around 11,000 cal BP. This indicates a reduction in the strength of near bottom currents on the Vøring plateau at this time. One possible cause is that the production of NADW moved south during this period or became less efficient due to the discharge of fresh water from glacial lakes in Canada (Fisher *et al.* 2002). Terrestrial data in Scandinavia indicate a cool period (Björck *et al.* 1997) between 11,300 and 11,150 cal BP, which is known as the Pre-Boreal Oscillation (PBO). This cooling event was widespread in the North Atlantic region (Björck *et al.* 1997). The timing of the reduction of NADW formation identified in MD95-2011 is significantly younger than the PBO (Björck *et al.* (1997).

After 11,000 cal BP, the bottom currents start to increase in intensity, as reflected by a coarser magnetic grain size in the sediment on the Vøring plateau. After 500 years there is a short decrease in magnetic grain size. After 10,000 cal BP the magnetic grain size slowly starts to increase in core MD95-2011, which reflects the start of Holocene Thermal Maximum (HTM) which lasted from 9,500 to 6,500 cal BP.

In the Norwegian Sea the HTM is seen as an increase of near bottom current speed. At 9,500 cal BP the current speed increased at the Vøring plateau. The rapid increase of near bottom currents after the 8.2 kyr cooling event is notable and it appears like there is a time lag over the Vøring plateau between SST and bottom current intensity. At 6,500 cal BP on the Vøring plateau the current strength started to slowly decrease and the magnetic grain size slowly decreased to.

Andersen *et al.* (2004) call the next period the Holocene Transition Period (HTP 6,500-3,000 cal BP), or alternatively the Holocene Cooling Period (HCP) (Birks & Koç 2002). The HTP or HCP is seen in MD95-2011 as a decrease in bottom current strength. The surface water actually started to cool from 7,230 cal BP (Birks & Koç 2002) in the Norwegian Sea and less warm surface water flowed north from the equatorial parts of the Atlantic Ocean. The bottom currents over the Vøring plateau start to decrease.

At 3,300 cal BP MD95-2011 shows a spike of fine magnetic grain sizes, which represents a short duration anomaly. It is clear that this anomaly represents the finest magnetic grain size measured in this core, and it can be correlated to a similarly short anomaly in composite core LO09-14. In their magnetic hysteresis study of MIS 2 & 3 sediments on the Reykjanes Ridge, Snowball and Moros (2003) noticed that Ash Zone II (age of c. 52 kyr BP) was characterised by notably fine magnetic grain sizes. Zillen *et al.* (2002) obtain a calendar year age of 3295 +/- 95 cal BP for the Hekla 3 tephra isochron in the North Atlantic region. Thus, it is possible that the magnetic hysteresis data obtained from LO09-14 and MD95-2011 have identified the position of the H3 tephra. However, to determine exactly what the layer is, further investigations are necessary.

After 3,000 cal BP, SST's are uncertain. Birks & Koç *et al.* (2002) call this period the Late Holocene Warming from 3000 to 0 cal BP and Andersen *et al.* (2004) calls it the Cool Late Holocene Period (3,000-0 cal BP). Core MD95-2011 shows an increase in magnetic grain size at the top of the core. It is possible that the increase in magnetic grain size seen in the top of the core

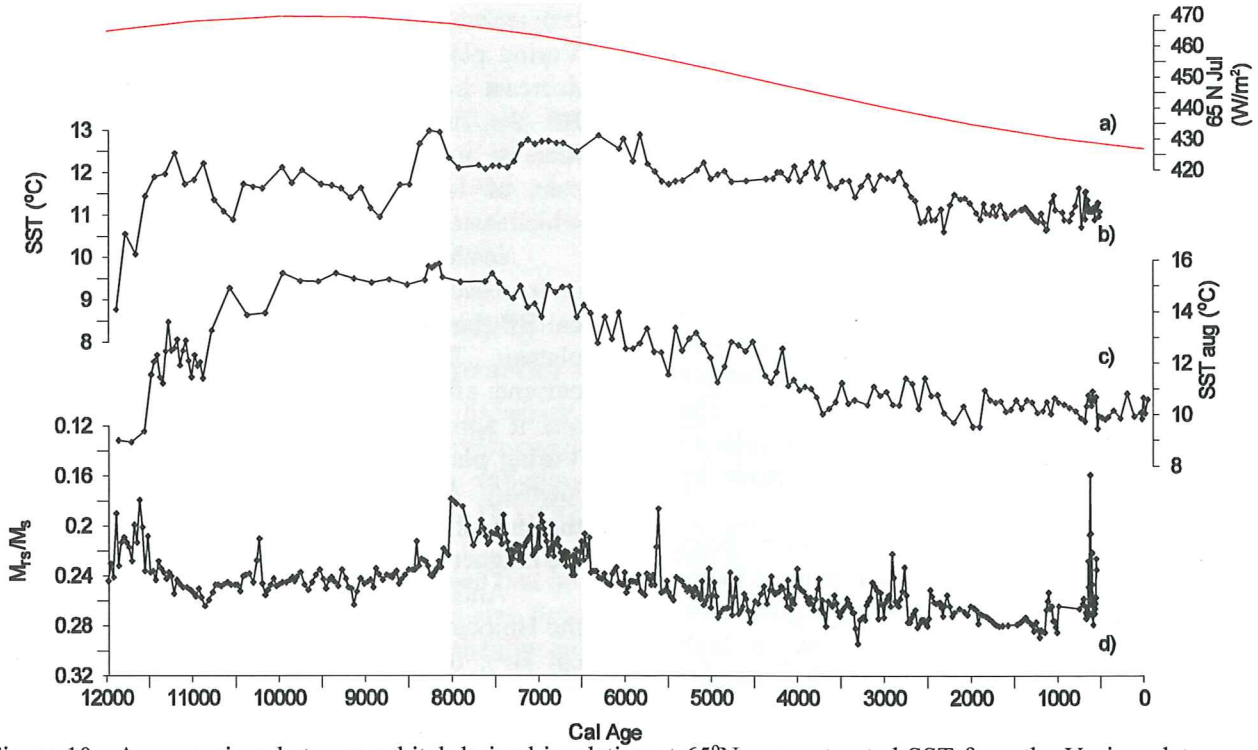


Figure 10. A comparison between orbital derived insolation at 65°N, reconstructed SST from the Vøring plateau and $M_{rs}/M_s$. Graph a) is the insolation curve from 65°N during July from Berger and Loutre (1991). b) The SST curve derived from $U^{K}_{37}$ is from Calvo *et al.* (2002). c) A SST reconstruction based on diatoms (Birks & Koç 2002). d) The magnetic ratio ($M_{rs}/M_s$) is interpreted as grain size variations (Vlag *et al.* 1996) in core MD95-2011. The shaded areas represent the period of coarse magnetic grain size in core MD95-2011.

is the Little Ice Age and due to an increase of IRD.

# 7 Conclusions

1. The magnetic hysteresis properties of the Holocene sediment cores analysed, from the North Atlantic and Norwegian seas, vary within and between cores.

2. The cause of the variation in magnetic properties may not be the same within and between cores. Thus, this study indicates that the hypothesis of a relation between magnetic grain size and near-bottom current flow intensity cannot be universally applied.

3. The magnetic hysteresis properties of samples taken from core MD95-2011 show a good correlation with reconstructed SST temperatures. In this case hydrological sorting is the most likely cause of the magnetic gain size variations, which implies that the maximum near bottom current flow speed occurred between 8,000 and 6,500 cal BP at this site. This period corresponds to the Holocene Thermal Maximum (Snowball *et al.* 2004).

4. A major change in the magnetic properties of sediments deposited at intermediate water depths on the Reykjanes Ridge occurred 3,000 cal BP. In this case the amplitude of the within core variation is similar to changes identified over D/O cycles during the last major Northern Hemisphere glaciation. However, unlike the D/O cycles, the wasp-waisted shape of the hysteresis loops precludes interpretation in terms of bottom current flow speed and rather indicates that there was a significant change in sediment source at 3,000 cal BP.

# 8 Acknowledgements

I want to thank my supervisors Ian Snowball and Matthias Moros for their comments and the discussions that have been very helpful in writing this project. I would also like to thank them for providing the data that has been used in this work. I would like to thank Ian Snowball for reviewing the language in the text. I also wish to thank the Geology Department at Lund University for genuine support from various sources. I also want to thank Martina Lundgren for the social support

and for the non-scientific comments that she has shared.

# 9 References

Andersen, C., Koç, N., Jennings, A. & Andrews, J. T., 2004: Nonuniform response of the major surface currents in the Nordic Seas to insolation forcing: Implications for the Holocene climate variability. *Paleoceanography 19,* 1–16.

Andrews, J. T., Hardardottir, J. Stoner, J. S., Mann, M. E., Kristjansdottir, G. B., & Koç, N., 2003: Decadal to millennial-scale periodicities in North Iceland shelf sediments over the last 12000 cal yr: long-term North Atlantic oceanographic variability and solar forcing. *Earth and Planetary Science Letters 210*, 453–465.

Berger, A., & Loutre, M. F., 1991: Insolation values for the climate of the last 10000000 years. *Quaternary Science Reviews 10*, 297–317.

Bianchi, G. G., & McCave, N. I., 1999: Holocene periodicity in North Atlantic climate and deep-ocean flow south of Iceland. *Nature 397*, 515–517.

Birks, C. J. A. & Koç, N., 2002: A high-resolution diatom record of late-Quaternary sea-surface temperatures and oceanographic conditions from the eastern Norwegian Sea. *Boreas 31*, 323–344.

Björck, S., Rundgren, M., Ingolfsson, O. & Funder, S., 1997: The Preboreal oscillation around the Nordic Seas: terrestrial and lacustrine responses. *Journal of Quaternary Science 12(6)*, 455–465.

Björck, S., Koç, N. & Skog, G., 2003: Consistently large marine reservoir ages in the Norwegian Sea during the Last Deglaciation. *Quaternary Science Reviews 22*, 429–435.

Bond, G., Showers, W., Cheseby, M., Lotti, R., Almasi, P., deMenocal, P., Priore, P., Cullen, H., Hajdas, I. & Bonani, G., 1997: A Pervasive Millennial-Scale Cycle in North Atlantic Holocene and Glacial Climates. *Science 278*, 1257–1266.

Bond, G., Kromer, B., Beer, J., Muscheler, R., Evans, M. N., Showers, W., Hoffman, S., Lotti-Bond, R., Hajdas, I. & Bonani, G., 2001: Persistent Solar Influence on North Atlantic Climate During the Holocene. *Science 294*, 2130–2136.

Broecker, W. S., 1998: Paleocean circulation during the last deglaciation: A bipolar seesaw. *Paleoceanography 13(2)*, 119–121.

Calvo, E., Grimalt, J. & Jansen, E., 2002: High resolution $U_{37}^{K}$ sea surface temperature reconstruction in the Norwegian Sea during the Holocene. *Quaternary Science Reviews 21*, 1385–1394.

Chapman, M. R. & Shackelton, N. J., 2000: Evidence of 550-year and 1000-year cyclicities in the North Atlantic circulation pattern during the Holocene. *The Holocene 10(3)*, 287–291.

Colman, S. M., Keigwin, L. D. & Forester, R. M., 1994: 2 episodes of meltwater influx from glacial lake Agassiz into the Lake-Michigan Basin and their climatic contrasts. *Geology 22(6)*, 547–550.

Day, R., Fuller, M. & Schmidt, V. A., 1977: Hysteresis properties of titanomagnetites: Grain-size and compositional dependence. *Physics of the Earth and Planetary Interiors 13(4)*, 260–267.

Denton, G. H. & Karlén, W., 1973: Holocene climatic variations; their pattern and possible cause. *Quaternary research3;2,* 155–205.

Fisher, T. G., Smith, D. G. & Andrews, J. T., 2002: Preboreal oscillation caused by glacial Lake Agassiz flood. *Quaternary Science Reviews 21*, 873–878.

Hammarlund, D., Björck, S., Buchardt, B., Israelson, C. & Thomsen, C. T., 2003: Rapid hydrological change during the Holocene revealed by stable isotope records of lacustrine carbonates from Lake Igelsjön, southern Sweden. *Quaternary Science Reviews 22*, 353–370.

Heinrich, H., 1988: Origin and Consequence of Cyclic Ice Rafting in the Northeast Atlantic Ocean during the past 130,000 years. *Quaternary Research 29*, 142–152.

Hurrell, J. W., Kushnir, Y. & Visbeck, M., 2001: The north Atlantic Oscillation. *Science 291*, 603–605.

Jiang, H., Svensson, N-O. & Björck, S., 1998: Meltwater Discharge to the Skagerrak-Kattegat from the Baltic Ice Lake during the Younger Dryas Interval. *Quaternary Research 49*, 264–270.

Johnsen, S. J., Dahl-Jensen, D., Gundestrup, N., Steffensen, J. P., Clausen, H. B., Miller, H., Masson-Delmotte, V., Sveinbjörnsdottir, A. E. & Withe, J., 2001: Oxygen isotope and palaeotemperature records from six Greenland ice-core stations: Camp Century, Dye-3, GRIP, GISP2, Renland and NorthGRIP. *Journal of Quaternary Science 16(4)*, 299–307.

Kissel, C., Laj, C., Labeyrie, L., Dokken, T., Voelker, A. & Blamart, D., 1999: Rapid climatic variations during marine isotopic stage 3: magnetic analysis of sediment from Nordic Seas and North Atlantic. *Earth and Planetary Science Letters 171*, 489–502.

Laj, C., Kissel, C., Mazaud, A., Michel, E., Muscheler, R. & Beer, J., 2002: Geomanetic field intensity, North Atlantic Deep Water circulation and atmospheric $\Delta^{14}C$ during the last 50 kyr. *Earth and Planetary Science Letters 200*, 177–190.

Larsen, E., Sejrup, H. P., Johnsen, S. J. & Knudsen, K. L., 1995: Do Greenland ice cores reflect NW European interglacial climate variations? *Quaternary Research 43*, 125–132.

Magny, M., Bégeot, C., Guiot, J. & Peyron, O., 2003: Contrasting patterns of hydrological changes in Europe in response to Holocene climate cooling phases. *Quaternary Science Reviews 22*, 1589–1596.

Martrat, B., Grimalt, J. O., Villanueva, J., van Kreveld, S. & Sarnthein, M., 2003: Climatic dependence of the organic matter contributions in the north eastern Norwegian Sea over the last 15,000 years. *Organic Geochemistry 34*, 1057–1070.

McCave, I. N., Manighetti, B. & Robinson, S. G., 1995: Sortable silt and fine sediments size composition slicing–parameters for paleocurrents speed and paleoceanography *Paleoceanography 10(3)*, 593–610.

Moros, M., Endler, R., Lackschewitz, K. S., Wallrabe-Adams H.-J., 1997: Physical properties of Reykjanes Ridge sediments and their linkage to high-resolution Greenland Ice sheet Project 2 ice core data. *Paleoceanography 12(5)*, 687–695.

Moros, M., Kuijpers, A., Snowball, I., Lassen, S., Bäckstöm, D., Gingele, F., & McManus, J., 2002: Were glacial iceberg surges in the North Atlantic triggered by climatic warming? *Marine Geology 192*, 393–417.

Moros, M., Emeis, K., Risebrobakken, B., Snowball, I., McManus, J. & Jansen, E., 2004: Sea surface temperatures and ice rafting in the Holocene North Atlantic: climate influences on northern Europe and Greenland. *Quaternary Science Reviews 23*, 2113–2126.

Pirrung, M., Fütter, D., Grobe, H., Matthiessen, J. & Niessen, F., 2002: Magnetic susceptibility and ice-rafted debris in surface sediments of the Nordic Sea: implications for Isotope Stage 3 oscillation. *Geo-Marine Letters 22*, 1–11.

Rasmussen, T. L., van Weering, T. C. E. & Labeyrie, L., 1996a: High resolution stratigraphy of the Faeroe-Shetland Channel and its relation to North Atlantic paleoceanography: the last 87 kyr. *Marine Geology 131*, 75–88.

Rasmussen, T. L., Thomsen, E., van Weering, T. C. E. & Labeyrie, L., 1996b: Rapid change in surface and deep water conditions at the Faeroe Margin during the last 58,000 years. *Paleoceanography 11(6)*, 757–771.

Rasmussen, T. L., van Weering, T. C. E. & Labeyrie, L., 1997: Climatic instability, ice sheet and ocean dynamics at high northern latitudes during the last glacial period (58-10 ka BP). *Quaternary Science Reviews 16*, 71–80.

Risebrobakken, B., Jansen, E., Andersson, C., Mjelde, E. & Hevrøy, K., 2003: A high-resolution study of Holocene paleoclimatic and paleoceanographic change in the Nordic Seas. *Paleoceanography 18(1)*, 1–17.

Robinson, S. G., Maslin, M. A. & McCave, N. I., 1995: Magnetic susceptibility variations in Upper Pleistocene deep-sea sediments of the NE Atlantic: Implications for ice rafting and paleocirculation at the last glacial maximum. *Paleoceanography 10(2)*, 221–250.

Sarnthein, M., van Kreveld, S., Erlenkeuser, H., Grootes P. M., Kucera, M., Pflaumann, U., & Schulz, M., 2003: Centennial-to-millennial periodicities of Holocene climate and sediment injections off the western Barents shelf, 75°N. *Boreas 32*, 447–461.

Sartori, M., Heller, F., Forster, T., Borkovec, M., Hammann, J. & Vincent, E., 1999: Magnetic properties of loess grain size fractions from the section at Paks (Hungary). *Physics of the Earth and Planetary Interiors 116*, 53–64.

Snowball, I. & Moros, M. 2003: Saw-tooth pattern of North Atlantic current speed during Dansgaard-Oeschger cycles revealed by the magnetic grain size of Reykjanes Ridge sediments at 59°N. *Paleoceanography 18(2)*, 1–11.

Snowball, I., Korhola, A., Briffa, K., R., & Koç, N., 2004: Past Climate Variability through Europe and Africa. *Academic Publishers,* Dordrecht, the Netherlands. s465–489 .

Stocker, T., F., 2000: Past and future reorganizations in the climate system. *Quaternary Science Reviews 19*, 301–319.

Stoner, J., S., Channell, J., E., T., & Hillaire-Maecel, C., 1996: The magnetic signature of rapidly deposited detrital layers from the deep Labrador Sea: Relationship to North Atlantic

Heinrich layers. *Paleoceanography 11(3)*, 309–325.

Thompson, R., & Oldfield, F., 1986: Environmental magnetism. *Allen and Unwin*, London, 1986.

Vlag, P., Rochette, P. & Dekkers, M. J., 1996: Some additional hysteresis parameters for a natural (titano)magnetite with known grain size. *Geophysical research letters 23(20)*, 2803–2806.

Watkins, S. J., & Maher, B. A., 2003: Magnetic Characterisation of present-day deep-sea sediments and sources in the North Atlantic. *Earth and Planetary Science Letters 214*, 379–394.

Zillén, L. M., Wastegård, S. & Snowball, I., 2002: Calendar year ages of three mid-Holocene tephra layers identi.ed in varved lake sediments in west central Sweden. *Quaternary Science Reviews 21*, 1583–1591.

**Tidigare skrifter i serien "Examensarbeten i Geologi vid Lunds Universitet":**

125. Kjöllerström, Anders, 2000: En geokemisk studie av bergartsvariationen på Bullberget i västra Dalarna.
126. Cinthio, Kajsa, 2000: Senglacial och tidigholocen etablering och expansion av lövträd på en lokal i nordvästra Rumänien.
127. Lamme, Sara, 2000: Klimat och miljöförändringar under holocen i Sylarnaområdet, södra svenska Skanderna, baserat på analys av makrofossil och klyvöppningar.
128. Jönsson, Charlotte, 2000: Geologisk och hydro-geologisk modellering av området mellan Bjuv och Söderåsen, nordvästra Skåne.
129. Kleman, Johan, 2001: Utvärdering av den underkambriska litostratigrafin på Österlen, södra Sverige.
130. Sundler, Malin, 2001: En jämförande studie mellan uppmätt och MACRO simulerad pesticidutlakning på ett odlingsfält i Skåne.
131. Grönholm, Anna, 2001: Högtrycksmetabasiter i den södra delen av Mylonitzonen: fältgeologi, petrografi och metamorf utveckling.
132. Ekdahl, Magnus, 2001: En studie av Källsjögranitens deformationsmönster och kinematiska indikatorer inom Ullaredszonen.
133. Axheimer, Niklas, 2001: Middle Cambrian trilobites and biostratigraphy of the Almbacken drill core, Scania, Sweden.
134. Lindén, Mattias, 2001: Proglacial deformation of glaciofluvial sediments during the Pomeranian deglaciation in the Neubrandenburg area, NE Germany.
135. Warnhag, Jon, 2001: A geochemical study of the zoned Pan African Mon Repos intrusion, Central Namibia.
136. Lundmark, Mattias, 2001: Zirkonstudie av Norra Hortens bergarter, SV Sverige.
137. Gunnarson, Rebecka, 2001: Sedimentologisk undersökning av en moränskärning i en djup-vittrad sprickdal på Romeleåsen, Skåne.
138. Karlsson, Christine, 2001: Diagenetic and petro-physical properties of deeply versus moderately buried Cambrian sandstones of the Caledonian foreland, southern Sweden.
139. Eriksson, Mårten, 2001: Bedömning av föroreningsspridning kring en nedlagd bensinstation i Karlaby, sydöstra Skåne.
140. Ljung, Karl, 2001: A paleoecological study of the Pleistocene Holocene transition in the Kap Farvel area, South Greenland.
141. Åkesson, Cecilia, 2001: Undersökning av grundvattenförhållanden i området kring Östra Vemmerlöv, Simrishamns kommun, sydöstra Skåne.
142. Bermin, Jonas, 2001: Modelling Mössbauer spectra of biotite.
143. Mansurbeg, Howri, 2001: Modelling of reservoir quality in quartz-rich sandstones of the Lower Cretaceous Bentheim sandstones, Lower Saxony Basin, NW Germany.
144. Hermansson, Tobias, 2001: Sierggavággeskollans strukturgeologiska utveckling; nyckeln till Sareks berggrundsgeologi.
145. Veres, Daniel-Stefan, 2001: A comparative study between loss on ignition and total carbon analysis on Late Glacial sediments from Atteköps mosse, southwestern Sweden, and their tentative correlation with the GRIP event stratigraphy.
146. Ahlberg, Tomas, 2001: Hydrogeologisk undersökning samt sårbarhetskartering av området kring tre bergborrade grundvattenanläggningar i Simrishamns kommun.
147. Boman, Daniel, 2001: Tektonostratigrafi och deformationsrelaterad metamorfos i norra Kebnekaisefjällen, Skandinaviska Kaledoniderna.
148. Olsson, Stefan, 2002: The geology of the Portobello Peninsula; proposal of a saturated to oversaturated lineage within the Dunedin Volcano, New Zealand.
149. Molnos, Imre, 2002: Petrografi och diagenes i den underkambriska lagerföljden i Skrylle, Skåne.
150. Malmborg, Pär, 2002: Correlation between diagenesis and sedimentary facies of the Bentheim Sandstone, the Schoonebeek field, The Netherlands.
151. Jonsson, Henrik, 2002: Permeability variation in a tidal Jurassic deposit, Höganäs basin, Fennoscandian Border Zone
152. Lundgren, Anders, 2002: Seveskollorna i nord-östra Kebnekaise, Kaledoniderna: metabasiter, graniter och ögongnejser.
153. Sultan, Lina, 2002: Reconstruction of fan-shaped outwash in front of the Mýrdalsjökull ice cap, Iceland: Architecture and style of sedimentation.
154. Rimša, Andrius, 2002: Petrological study of the metamafic rocks across the Småland-

Blekinge Deformation Zone

155. Lund, Magnus, 2002: Anti-slope scarp investigation at Handcar Peak, British Columbia, Canada.
156. Sjöstrand, Lisa: 2003: Early to early Middle Ordovician conodont biostratigraphy of the Tamsalu drill core, central Estonia.
157. Nilsson, Jonas, 2003: Carcharhiniforma hajar från Limhamns kalkbrott.
158. Larsson, Linda M., 2003: Late Triassic and Early Jurassic palynology of the Höganäs Basin and the Ängelholm Trough, NW Scania, Sweden.
159. Sköld, Pia, 2003: Holocen skogshistoria i Stenshuvuds nationalpark, Skånes östra kust, Sverige.
160. Fuchs, M., 2003: Påverkan av sterilisering på gruvsand – en mineralogisk och texturell undersökning.
161. Ljungberg, Julia, 2003. Sierggavággeskollan i gränslandet mellan Sarek och Padjelanta; miljöindikatorer för fjällkedjeberggrundens bildning.
162. Håkansson, Lena, 2003: An architectural element analysis of a large-scale thrust complex, Kanin Peninsula, NW Russia: interaction between the Barents and Kara Sea ice sheets.
163. Davidson, Anja, 2003: Ignimbritenheterna i Barranco de Tiritaña, övre Mogánformationen, Gran Canaria.
164. Näsström, Helena, 2003: Klotdioriten vid Slättemossa, centrala Småland – mineralkemi och genes.
165. Nilsson, Andreas, 2003: Early Ludlow (Silurian) graptolites from Skåne, southern Sweden.
166. Dou, Marion, 2003: Les ferromagnésiens du granite rapakivique de Nordingrå – centre-est de la Suède – composition chimique et stade final de cristallisation.
167. Jönsson, Emma, 2003: En pollenanalytisk studie av råhumusprofiler från Säröhalvön i norra Halland.
168. Alwmark, Carl, 2003: Magmatisk och metamorf petrologi av en mafisk intrusion i Mylonitzonen.
169. Pettersson, Ann, 2003: Jämförande litologisk och geokemisk studie av Sevens amfibolitkomplex i Sylarna och Kebnekaise.
170. Axelsson, Katarina, 2004: Bedömning av potentiell föroreningsspridning från ett avfallsupplag utanför Löddeköpinge, Skåne.
171. Ekestubbe, Jonas, 2004: $^{40}Ar/^{39}Ar$ geokronologi och implikationer för tolkningen av den Kaledoniska utvecklingen i Kebnekaise.
172. Lindgren, Paula, 2004. Tre sensvekofenniska graniter: kontakt- och åldersrelationer samt förekomst av metasedimentära enklaver.
173. Janson, Charlotta, 2004. A petrographical and geochemical study of granitoids from the south-eastern part of the Linderödsåsen Horst, Skåne.
174. Jonsson, Sara, 2004: Structural control of fine-grained granite dykes at the Äspö Hard Rock Laboratory, north of Oskarshamn, Sweden.
175. Ljungberg, Carina, 2004: Belemniters stabila isotopsammansättning: paleomiljöns och diagenesens betydelse.
176. Oster, Jessica, 2004: A stratigraphic study of a coastal section through a Late Weichselian kettle hole basin at Ålabodarna, western Skåne, Sweden.
177. Einarsson, Elisabeth, 2004: Morphological and functional differences between rhamphorhynchoid and pterodactyloid pterosaurs with emphasis on flight.
178. Anell, Ingrid, 2004: Subsidence in rift zones; Analyzing results from repeated precision leveling of the Vogar Profile on the Reykjanes Peninsula, Southwest Iceland.
179. Wall, Torbjörn, 2004: Magnetic grain-size analyses of Holocene sediments in the North Atlantic and Norwegian Sea – palaeoceano-graphic applications.

LUNDS UNIVERSITET

Geologiska institutionen
Gentrum för GeoBiosfärsvetenskap
Sölvegatan 12, 223 62 Lund